KeAi

CHINESE ROOTS
GLOBAL IMPACT

Contents lists available at ScienceDirect

Petroleum Science

journal homepage: www.keaipublishing.com/en/journals/petroleum-science



Original Paper

Effects of different thermal insulated drill pipe deployment methods on wellbore temperature control in ultra-deep wells



Heng-Rui Zhang ^{a,b}, Yi-Nao Su ^{a,b,c}, Mao-Lin Liao ^{a,b,*}, Hong-Yu Wu ^{a,b}, Hai-Yan Zhang ^{a,b}, Hao-Yu Wang ^{a,b}, Ke Liu ^c

- ^a Downhole Intelligent Cybernetics Institute, University of Science and Technology Beijing, Beijing, 100083, China
- ^b School of Mechanical Engineering, University of Science and Technology Beijing, Beijing, 100083, China
- ^c China National Petroleum Corporation Engineering Technology R&D Company Limited, Beijing, 102206, China

ARTICLE INFO

Article history: Received 13 November 2024 Received in revised form 8 September 2025 Accepted 8 September 2025 Available online 12 September 2025

Edited by Jia-Jia Fei

Keywords:
Ultra-deep wells
Thermal insulated drill pipe
Wellbore temperature control
Deployment methods
Numerical simulation

ABSTRACT

The exploitation of oil resources has now extended to ultra-deep formations, with depths even exceeding 10,000 m. During drilling operations, the bottomhole temperature (BHT) can surpass 240 °C. Under such high-temperature conditions, measurement while drilling (MWD) instruments are highly likely to malfunction due to the inadequate temperature resistance of their electronic components. As a wellbore temperature control approach, the application of thermal insulated drill pipe (TIDP) has been proposed to manage the wellbore temperature in ultra-deep wells. This paper developed a temperature field model for ultra-deep wells by coupling the interactions of multiple factors on the wellbore temperature. For the first time, five distinct TIDP deployment methods were proposed, and their corresponding wellbore temperature variation characteristics were investigated, and the heat transfer laws of the ultra-deep wellbore-formation system were quantitatively elucidated. The results revealed that TIDP can effectively restrain the rapid rise in the temperature of the drilling fluid inside the drill string by reducing the heat flux of the drill string. Among the five deployment methods, the method of deploying TIDP from the bottomhole upwards exhibits the best performance. For a 12,000 m simulated well, when 6000 m of TIDP are deployed from the bottomhole upwards, the BHT decreases by 52 °C, while the outlet temperature increases by merely 1 °C. This not only achieves the objective of wellbore temperature control but also keeps the temperature of the drilling fluid at the outlet of annulus at a relatively low level, thereby reducing the requirements for the heat exchange equipment on the ground. The novel findings of this study provide significant guidance for wellbore temperature control in ultra-deep and ultra-high-temperature wells.

© 2025 The Authors. Publishing services by Elsevier B.V. on behalf of KeAi Communications Co. Ltd. This is an open access article under the CC BY-NC-ND license (http://creativecommons.org/licenses/by-nc-nd/4.0/).

1. Introduction

The exploration and development of oil and gas resources have advanced into ultra-deep formations exceeding 10,000 m. At these depths, the near-well region experiences ultra-high temperatures surpassing 240 $^{\circ}$ C, causing the rapid heating of circulating drilling fluids. This intense heat renders existing downhole tools, working fluids, and measuring instruments inadequate to meet the high-

E-mail address: liaomaolin@ustb.edu.cn (M.-L. Liao).

Peer review under the responsibility of China University of Petroleum (Beijing).

temperature demands of ultra-deep wells, severely hampering drilling efficiency and compromising the stability of real-time data acquisition. Globally, numerous ultra-deep drilling operations have encountered downhole equipment failures and wellbore safety challenges due to the extreme wellbore temperatures. Countries such as China, the United States, Russia, and Germany are expending substantial efforts and resources to enhance the high-temperature tolerance of drilling systems, along with an escalating demand for improved temperature resilience in downhole tools, working fluids, and measuring instruments. However, the current progress in materials science and electronic information technologies has imposed constraints on the high-temperature tolerance of downhole equipment, leaving it insufficient to meet the actual needs of ultra-deep exploration and

^{*} Corresponding author.

development. To enable the routine application of conventional drilling technologies in ultra-deep wells, it is crucial to control the wellbore temperature. By lowering the temperature of the drilling fluid circulating in the wellbore to a level compatible with existing downhole equipment, conventional drilling technologies and equipment could operate effectively in the extreme temperature environment of ultra-deep wells.

In the drilling process, wellbore temperature control usually relies on natural cooling and low-temperature medium mixing methods on the ground. However, in ultra-deep wells, there is a large interaction area between the wellbore-wall and the adjacent formation. The high formation temperature impacts the circulating fluid in the annular region of the wellbore, where heat from the high-temperature annulus is conducted within the drill string. This results in a rapid temperature increase in the drilling fluid as it flows toward the bottomhole, rendering ground-based cooling less effective for wellbore temperature control. Given the difficulty in controlling heat transfer between the annulus and the adjacent formation through the wellbore-wall, and the current limitations of related technologies, a novel approach is necessary to achieve effective temperature control. This study proposes a wellbore temperature control method utilizing thermal insulated drill pipe (TIDP), which have ultra-low thermal conductivity, deployed in the downhole drill string system. By the deployment of TIDP in downhole drill string system, heat transfer from the annulus to the interior of the drill string is reduced, thereby suppressing the rapid temperature rise of the drilling fluid as it travels from the wellhead to the bottom. This ensures that the wellbore temperature remains within the safe operating range for existing temperature-sensitive instruments and measurement equipment.

The drill pipe insulation technology research conducted by the U.S. Department of Energy (DOE) on geothermal drilling represents a significant milestone in the development of drill pipe insulation technology. In the early 21st century, Sandia National Laboratories, in collaboration with Drill Cool Systems, first proposed a downhole drill string insulation solution involving welding liners inside the drill pipe and filling them with insulating materials, which reduced the thermal conductivity of the drill pipe from 43.3 to 3.35 W/(m·K). Based on this insulated drill pipe, initial field tests were conducted (Finger et al., 2002). With the continuous advancement of drilling technology, the U.S. DOE conducted field tests on insulated drill pipes at a 2657 m geothermal well in the Utah FORGE project in 2023. The thermal conductivity of the insulated drill pipes employed in the field test was 3.12 W/(m·K). The test results indicated that for the Utah FORGE geothermal well, the use of TIDP significantly reduced the bottomhole temperature (BHT). Compared to conventional drill pipe (CDP), BHT was reduced by 14%-44%, and the cooling effect was more pronounced in deeper wells (Mohamed et al., 2023).

To ensure both the safety and economic feasibility of TIDP deployment in drilling engineering applications, it is necessary to develop a wellbore temperature field model for ultra-deep wells and propose a systematic and appropriate method for deploying TIDP in the drill string system, and thus to determine the optimal quantity and well section locations for the TIDP application. Research on the development of wellbore temperature field models has transitioned from simple to increasingly complex models. In 1937, Schlumberger et al. emphasized the necessity of fluid temperature prediction in their study on wellbore fluid temperature testing (Schlumberger et al., 1934). With the support of advancements in computational technology, since the 1960s, numerous researchers have conducted studies on wellbore temperature fields in oil and gas drilling, proposing various theories and methods for calculating wellbore temperature distribution. Edwardson et al. (1962), Ramey (1962), and Raymond (1969)

established foundational models for predicting transient and steady-state wellbore temperature profiles. Subsequently, Kabir, Hasan, and others (Hasanand Kabir, 1992; Kabir et al., 1996) optimized these foundational wellbore temperature field models by considering multiphase flow, transient/steady-state conditions, and diverse operational scenarios. With the growing complexity of drilling conditions and the diversification of drilling methods. scholars have developed steady-state and transient temperature prediction models for various drilling processes, including horizontal well drilling (Yang et al., 2022a; An et al., 2023), deepwater drilling (Song and Guan, 2011; Mao et al., 2023), deep shale gas horizontal well drilling (Fu et al., 2019), deep shale underbalanced drilling (Zhang et al., 2023), coiled tubing drilling (Wang et al., 2011), phase-change material temperature-controlled drilling (Zhang et al., 2025), and high-temperature and high-pressure wells (Wang et al., 2019; Peng et al., 2016).

The research on the wellbore temperature field when considering the application of drill pipe insulation mainly began in 2022. Xiao et al. proposed a heat extraction technology method during drilling that combines the TIDP with the phase change heat storage materials. This method effectively reduces the BHT while utilizing the geothermal energy of high-temperature wells (Xiao et al., 2022a). In the same year, Xiao et al. established a transient model of the temperature distribution in the wellbore during deep shale gas wells drilling in the horizontal well section, studied the influences of the circulation time, rate of penetration, inlet temperature, and thermal conductivity of the drill pipe, etc. on the wellbore temperature distribution, and verified that the TIDP is the most effective measure for cooling the wellbore (Xiao et al., 2022b). In 2023, Kohei et al. took into account the flow velocity and inflow temperature of the circulating fluid, numerically simulated the additional pressure loss that the insulated drill pipe may bring to the circulating fluid, and studied the changes in the wellbore temperature when the TIDP is only used in some well sections (Kohei et al., 2023). In 2024, Song et al. constructed a transient heat transfer model of the ultra-deep wellbore-formation considering the influence of the insulated coating inside the drill pipe according to the thermal conductivity characteristics of the insulated coating and the drill pipe, and revealed the influence law of the insulated coating on the temperature field of the ultradeep wellbore (Song et al., 2024). In the same year, Xiao et al. preliminarily explored the influence of the length and installation position of the TIDP on the wellbore temperature, and studied the detailed method of low-grade heat energy utilization during horizontal well drilling (Xiao et al., 2024).

Published research indicates that existing wellbore temperature field studies mainly focus on different drilling techniques, rather than conducting targeted research on the complex downhole conditions (such as fluid environment changes and multiple heat sources) in ultra-deep wells, especially those exceeding 10,000 m, and the heat transfer laws of drill strings and wellbores in long well sections. This limits their application in accurately simulating wellbore temperature changes and characterizing wellbore heat transfer characteristics. Although Xiao's team has done extensive work on TIDP, their research mainly focuses on the economic evaluation of drill pipe thermal insulation technology, and no targeted TIDP deployment scheme has been formed. The novelty of this study lies in its systematic analysis of multiple influencing factors of the circulating fluid temperature, coupling the characteristics between temperature field changes and heat exchange amounts in different downhole regions. Thus, a mathematical model suitable for calculating the wellbore temperature in ultra-deep well drilling is established. Additionally, five types of TIDP deployment methods (full-well deployment, top-down deployment, bottom-up deployment, sectional deployment, and

dual-end deployment) in the drill string system are proposed for the first time. Their corresponding changes in wellbore temperature field, heat transfer characteristics, and the advantages and disadvantages in drilling applications are analyzed and compared to optimize an effective TIDP deployment method. This work provides guidance for wellbore temperature control using TIDP in ultra-deep and ultra-high-temperature drilling environments.

2. Physical model

2.1. Analysis of the drilling process

Based on actual drilling conditions, this section constructs a physical model of the wellbore temperature field for ultra-deep wells, as shown in Fig. 1. The drilling fluid is injected from the ground within the drill string and flows downward towards the bottomhole. At the bottom, the drilling fluid inside the drill string enters the annulus through the nozzles of the rotating drill bit. In the annulus, the fluid flows from the bottomhole to the wellhead and returns to the surface through the annulus outlet. After undergoing a series of cooling and chemical treatment processes at the surface, the fluid is reinjected into the drill string, commencing the next circulation cycle.

During the aforementioned circulation process, highly complex flow-solid interface convective heat transfer, heat conduction, and frictional heat generation occur simultaneously within the wellbore. Specifically, heat exchange between the fluid inside the drill string and the annular fluid occurs through the drill string system, while heat transfer between the annular fluid and the adjacent formation

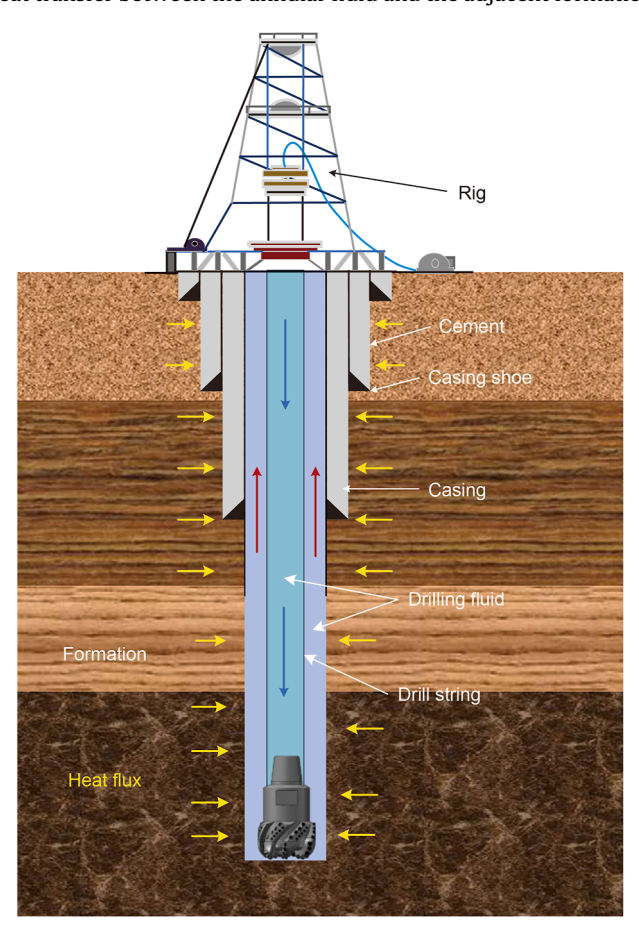


Fig. 1. Schematic diagram of the physical model for the wellbore temperature field in ultra-deep wells.

is conducted through the wellbore-wall. Additionally, during rock-breaking operations, the drill bit cutters generate substantial heat due to frictional interactions with the rock, while frictional heat is generated as the drilling fluid contacts the wellbore-wall (formation or casing) and the drill string during its circulation.

2.2. Model assumptions and discussion

To establish a physical model for the wellbore temperature field in ultra-deep wells, the actual operating conditions are transformed into a mathematical model. The following assumptions are made:

- (1) The formation is assumed to be radially symmetric, with the temperature remaining uniform at any radial distance from the wellbore axis.
- (2) The radial movement of the drilling fluid is disregarded, and the fluid flow within the wellbore is assumed to be one-dimensional axial flow. Moreover, the compressibility of the liquid-phase fluid is ignored.
- (3) To balance computational accuracy and efficiency of the developed model, the thermal properties of the drilling fluid are considered to be influenced exclusively by environmental temperature and pressure.
- (4) A thermal boundary exists in the radial direction of the wellbore, and the temperature at this boundary is assumed to stay equal to the original formation temperature (OFT), unaffected by the wellbore temperature changes.
- (5) The formation temperature gradient is assumed to be constant, and the thermal contact between the formation and the wellbore-wall is regarded as ideal, without any thermal contact resistance or temperature loss.
- (6) The differences in thermal conductivity between the drill bit and the drill pipe are neglected. Given the relatively small size of the drill bit, axial heat conduction at the drill bit position is not taken into account.
- (7) It is assumed that the comprehensive service performance of the TIDP is stable during the long-period drilling process, namely, the heat insulation effect does not deteriorate or fail due to the harsh downhole environment.

2.3. TIDP deployment methods

Compared to CDP, TIDP entails more intricate manufacturing processes and higher production costs. In oil and gas well drilling, to strike an optimal balance between the economic efficiency of drilling operations and the wellbore temperature control requirements, it is imperative to devise the TIDP deployment strategy and perform simulation analysis so as to determine the ideal arrangement and quantity of TIDP. This is crucial to avert excessive wellbore cooling, which could give rise to escalated material and economic costs. This study delves into diverse combinations of TIDP and CDP within the downhole drill string system and presents five distinct TIDP deployment methods:

- Full-well deployment of TIDP (Method A);
- TIDP deployment from the wellhead downwards to a specified depth range (Method B);
- TIDP deployment from the bottomhole upwards to a specified depth (Method C);
- Sectional deployment of TIDP (Method D);
- Deployment of TIDP at both ends of the drill string (Method E).

The five deployment methods are shown in Fig. 2.

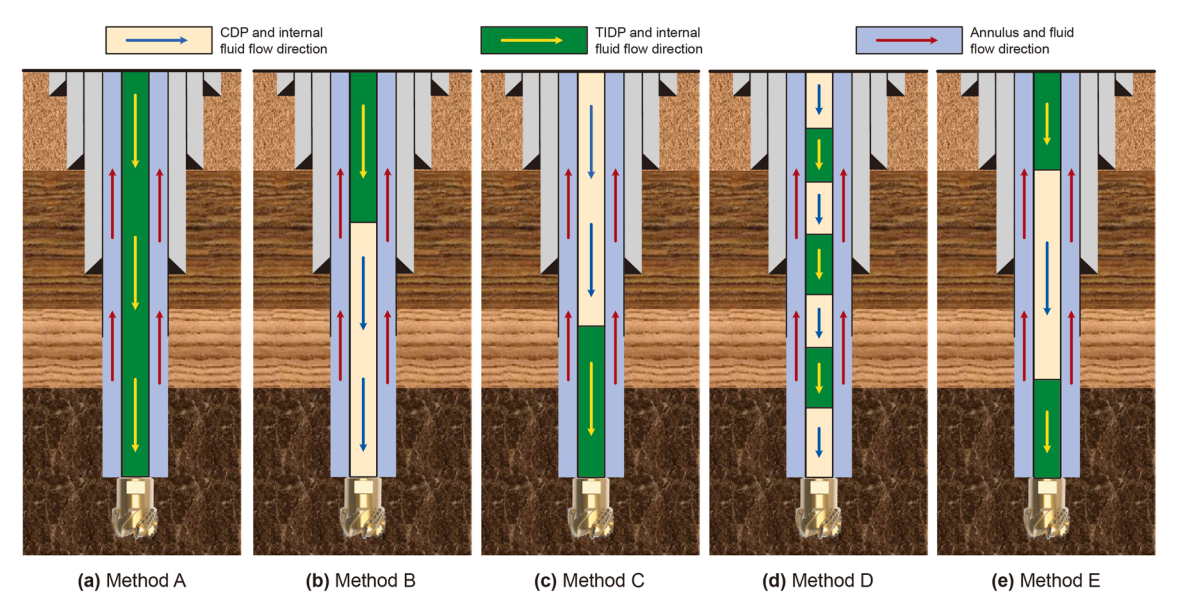


Fig. 2. Five TIDP deployment methods. (a) Method A, (b) Method B, (c) Method C, (d) Method D, (e) Method E.

2.4. Control volume setting for the model

In the physical model, the wellbore and the adjacent formation are divided into four regions: the interior of the drill string, the drill string, the annulus, and the adjacent formation. For the sake of convenient description, a control volume P is chosen within each region as the research subject. The four boundaries of control volume P are denoted as e, s, w and n, which respectively correspond to the east, south, west, and north boundaries. The four neighboring control volumes in the east, south, west, and north directions are designated as E, S, W, and N, respectively. The relationship between control volume P and the surrounding control volumes is shown in Fig. 3.

3. Mathematical model

3.1. Energy equations for different regions

3.1.1. Energy equation for drilling fluid inside the drill string

The temperature variation of the drilling fluid within the drill string is influenced by three key factors: the axial heat conduction of the drilling fluid, the heat transfer between the drilling fluid and the drill pipe, and the frictional heat generated during the interaction between the drilling fluid and the wellbore-wall. A control volume element of the circulating drilling fluid inside the drill string is selected, and its energy equation in differential form is formulated as presented in Eq. (1).

$$\begin{split} \pi r_{\mathrm{pi}}^2 \frac{\partial}{\partial t} (c \rho T_{\mathrm{in}}) &= -\pi r_{\mathrm{pi}}^2 \frac{\partial}{\partial z} (c \rho \nu_{\mathrm{i}} T_{\mathrm{in}}) + 2\pi r_{\mathrm{pi}} h_{\mathrm{pi}} (T_{\mathrm{in}} - T_{\mathrm{p}}) \\ &+ \frac{1}{4} \pi r_{\mathrm{pi}} f_{\mathrm{s}} \rho \nu_{\mathrm{in}}^3 \end{split} \tag{1}$$

In the heat source term of the aforementioned equation, the friction factor can be determined using the Hagen-Poiseuille equation (Qiu et al., 2021). For laminar flow (Re < 2300):

$$f_{\rm S} = \frac{64}{Re} \tag{2}$$

Under laminar flow conditions, the friction factor exhibits an inverse proportional relationship with the Reynolds number.

For turbulent flow (Re > 4000), the turbulent flow friction factor f_s can be determined by applying the Colebrook-White equation (Saeed, 2012). Nevertheless, since this equation is in an

implicit form, solving for f_s necessitates an iterative approach. To streamline the calculation process, this study employs an approximate solution to the Colebrook equation, namely the Swamee-Jain equation (Swamee and Jain, 1976), to compute the friction factor for turbulent pipe flow.

$$f_{\rm S} = \frac{0.25}{\left[\lg\left(\frac{\epsilon/D_{\rm h}}{3.7} + \frac{5.74}{Re^{0.9}}\right)\right]^2} \tag{3}$$

3.1.2. Energy equations for the drill string system

The energy equations for the drill string system comprise two parts: the energy equation for the drill string and that for the drill bit. The temperature variation in the drill string is affected by axial and radial heat conduction, and its energy equation is formulated as shown in Eq. (4).

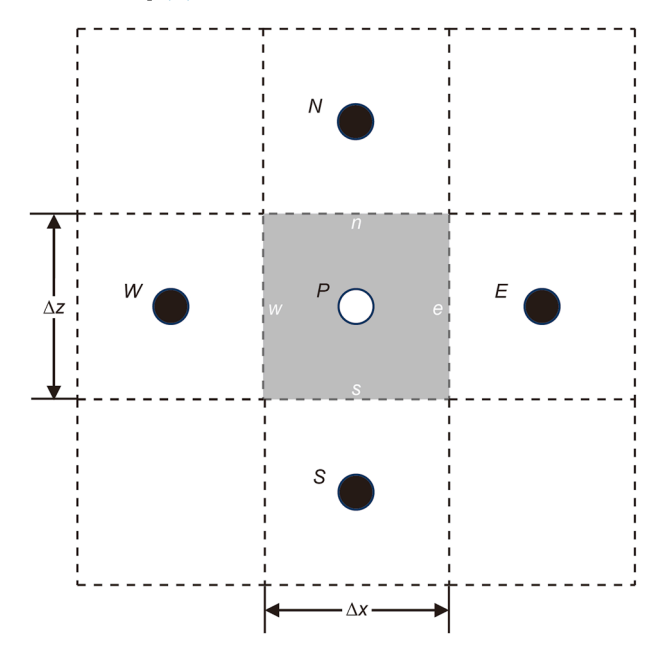


Fig. 3. Relationship between control volume P and surrounding control volumes.

$$\pi \left(r_{po}^{2} - r_{pi}^{2}\right) c_{p} \rho_{p} \frac{\partial T_{p}}{\partial t} = \pi \left(r_{po}^{2} - r_{pi}^{2}\right) k_{p} \frac{\partial^{2} T_{p}}{\partial z^{2}} + 2\pi \left[r_{po} h_{po} \left(T_{a} - T_{p}\right) - r_{pi} h_{pi} \left(T_{p} - T_{in}\right)\right]$$

$$(4)$$

Regarding heat transfer in the drill bit, in accordance with the assumptions, the thermal conductivity of the drill bit is considered the same as that of the drill string system. Analogous to the energy conservation equation for the drill string system, the internal fluid channel of the drill bit is in direct contact with the drilling fluid, while the outer shell of the drill bit is in contact with the drilling fluid in the annulus. Its temperature variation is determined by two factors: the radial heat conduction of the drill bit and the frictional heat generated during the interaction between the drill bit and the formation. As a result, the energy conservation equation for the drill bit is presented as shown in Eq. (5).

$$\pi \left(r_{po}^{2} - r_{pi}^{2}\right) c_{p} \rho_{p} \frac{\partial T_{p}}{\partial t} = \pi \left(r_{po}^{2} - r_{pi}^{2}\right) k_{p} \frac{\partial^{2} T_{p}}{\partial z^{2}} + 2\pi \left[r_{po} h_{po} \left(T_{a} - T_{p}\right) - r_{pi} h_{pi} \left(T_{p} - T_{in}\right)\right] + Q_{rg}$$

$$(5)$$

3.1.3. Energy equation for the circulating fluid in the annulus

Upon exiting the drill bit nozzles, the drilling fluid in the annulus travels from the bottomhole to the wellhead. During this flow journey, the drilling fluid comes into contact with the outer wall of the drill string system and the wellbore-wall (either the inner wall of the casing or the formation rock). Consequently, the temperature change of the fluid in the annulus is mainly governed by three factors: the axial heat conduction of the drilling fluid, the radial heat transfer between the annular drilling fluid and both the drill string and the wellbore-wall, and the frictional heat generated as the fluid flows along the wall surfaces. A control volume element of the annular drilling fluid is chosen, and its energy conservation equation is formulated as presented in Eq. (6).

$$\pi \left(r_{ci}^{2} - r_{po}^{2}\right) \frac{\partial}{\partial t} (c\rho T_{a}) = \pi \left(r_{ci}^{2} - r_{po}^{2}\right) \frac{\partial}{\partial z} (c\rho v_{a} T_{a})$$

$$+ 2\pi \left[r_{ci} h_{ci} \left(T_{f} - T_{a}\right) - r_{po} h_{po} \left(T_{a} - T_{p}\right)\right]$$

$$+ \frac{1}{4} \pi \left(r_{po} + r_{pi}\right) f_{s} \rho v_{a}^{3}$$

$$(6)$$

3.1.4. Energy conservation equation for the near-well formation

The inner wall of the near-well formation interfaces with the casing, whereas its outer wall directly adjoins the adjacent formation. The temperature change is influenced by two key factors: axial heat conduction and radial heat conduction within the formation. In accordance with the principle of energy conservation, the energy equation for this control volume can be articulated as the alteration in the control volume's internal energy being dictated by both axial and radial heat conduction processes within the formation. The energy equation is presented as depicted in Eq. (7).

$$\pi \left(r_{\rm f}^2 - r_{\rm ci}^2\right) c_{\rm f} \rho_{\rm f} \frac{\partial T_{\rm f}}{\partial t} = \pi \left(r_{\rm f}^2 - r_{\rm ci}^2\right) k_{\rm f} \frac{\partial^2 T_{\rm f}}{\partial z^2} + 2\pi \left[r_{\rm f} k_{\rm f} \left(T_{\rm OFT} - T_{\rm f}\right) - r_{\rm ci} k_{\rm c} \left(T_{\rm f} - T_{\rm a}\right)\right]$$

$$(7)$$

3.2. Model discretization and solution method

The solution is derived by integrating spatial steps within temporal intervals. The temporal grid corresponds to the predefined total circulation time, while the spatial grid is a two-dimensional mesh spanning the well depth and perpendicular radial directions. The mesh intervals along the well depth extend from the wellhead to the bottomhole, and the radial grid extends outward to infinity. The axial grid uses uniform step sizes, whereas the radial grid employs a non-uniform mesh (Fig. 4).

For the uniform axial mesh, conventional models typically utilize a fixed number of axial grids. When performing calculations for both shallow and deep well sections, the substantial variation in the total axial length (i.e., well depth) gives rise to fluctuations in grid resolution, which may potentially result in significant computational errors. In the present model, taking into account the distinctive features of ultra-deep well drilling, the number of uniform axial grids is adaptively adjusted in real-time according to different well depths during the computational process. This approach guarantees a consistently high level of precision in axial calculations. Regarding radial grid division, conventional models commonly adopt a fixed number of radial grids. Nevertheless, the temperature distribution within the drill string and the annulus, regions situated close to the wellbore axis, represents the focal point in solving the wellbore-formation temperature field. Conversely, the temperature field in areas farther away from the wellbore does not demand highly precise solutions. In this model. in order to achieve a balance between the emphasis on radial temperature field computations and the requirement for computational efficiency, non-uniform grids are employed for radial mesh division. Specifically, the grid becomes increasingly sparse as it extends further from the wellbore axis and progressively denser as it approaches the axis. In the simulation study of this paper, the initial number of axial grids is set as n = 400, and the number of radial grids is set as m = 15. Such treatment of the axial and radial grids effectively strikes an optimal balance between computational accuracy and speed, thereby producing the most comprehensive and accurate solution for the wellbore and adjacent formation temperature field.

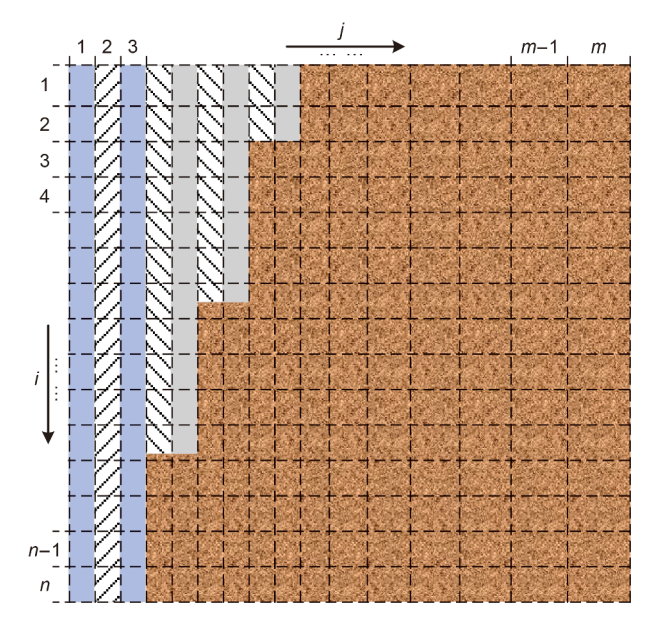


Fig. 4. Spatial grid division of the wellbore and near-well formation.

When solving the wellbore temperature field, the mathematical model should closely mimic the actual field conditions. In this research, the finite difference method is applied to solve the model. To ensure stability, the time term is handled using a fully implicit scheme. For the approximation of the first-order spatial derivative, a second-order upwind scheme is employed, which integrates information from two upstream points in the flow direction to enhance accuracy and minimize numerical diffusion. As for the second-order spatial derivatives, a three-point central difference scheme is utilized to boost the precision of heat conduction calculations and maintain numerical stability.

Upon the completion of equation discretization, the discrete energy equations for various regions of the wellbore and formation can be consolidated into Eq. (8) and presented in the form of a generalized vector, as illustrated in Eq. (9).

$$\alpha_{i,j} T_{i,j}^{t+\Delta t} - \beta_{i,j} T_{i,j}^{t} = \delta_{i-2,j} T_{i-2,j}^{t+\Delta t} + \varphi_{i-1,j} T_{i-1,j}^{t+\Delta t} + \gamma_{i+1,j} T_{i+1,j}^{t+\Delta t} + \varepsilon_{i+2,j} T_{i+2,j}^{t+\Delta t} + \eta_{i,j-2} T_{i,j-2}^{t+\Delta t} + \theta_{i,j-1} T_{i,j-1}^{t+\Delta t} + \sigma_{i,j+1} T_{i,j+1}^{t+\Delta t} + \xi_{i,j+2} T_{i,j+2}^{t+\Delta t} + b_{i,j}$$

$$(8)$$

$$\mathbf{A}\mathbf{T}^{n+1} = \mathbf{b} \tag{9}$$

Based on the aforementioned equations, the model can be solved by means of the Gauss-Seidel method (Yang et al., 2022b). To keep the description concise, the details of this method will not be elaborated upon in this context.

3.3. Auxiliary equations

3.3.1. Calculation method for formation temperature

Typically, the formation temperature escalates with the increase in formation depth, and the geothermal gradient serves as a means to quantify the rate of temperature change within the Earth's interior. This geothermal gradient value exhibits significant spatial variability across different regions. In accordance with the definition of the geothermal gradient, it is assumed that formations at the same vertical depth from the surface share an identical temperature. Presently, ultra-deep wells with depths exceeding 10,000 m are predominantly drilled with vertical well sections. During the drilling process, as the wellbore penetrates through diverse formation types, the geothermal gradients of these formations can differ substantially. To precisely characterize the original temperature of the formations encountered during drilling operations, the formation temperature can be described in Eq. (10):

$$T = T_{\text{surface}} + G_1 \int_0^{L_1} \cos \alpha_1 dl + G_2 \int_0^{L_2} \cos \alpha_2 dl + \dots + G_i \int_0^{L_i} \cos \alpha_i dl + \dots + G_n \int_0^{L_n} \cos \alpha_n dl$$

$$(10)$$

3.3.2. Calculation method for convective heat transfer coefficient

The convective heat transfer coefficient is of crucial importance in the heat transfer calculations within the drill string system. It is associated with the Nusselt number, thermal conductivity, and hydraulic diameter. The relevant equation is presented as follows (Fénot et al., 2011):

$$h = \frac{\lambda \cdot Nu}{D_{\rm h}} \tag{11}$$

In Eq. (11), Nu is closely related to the flow state of the circulating fluid and the geometry of the flow path. Its calculation generally relies on empirical formulas. For the circulating fluid

inside the drill string, the values of *Nu* under laminar and turbulent flow conditions are computed based on the relationship models put forward by Petersen et al. (2001) and Rao (2000). As for the circulating fluid in the annulus, the value of *Nu* is derived using the relationship models proposed by Michaelides (2006) and Fénot et al. (2011).

3.3.3. Calculation method for heat generation by the drill bit

The frictional heat produced by the drill bit during rock-breaking operations is calculated with the formula proposed by Memarzadeh and Stefan (1984) for PDC drill bits, as depicted in Eq. (12). This formula comprehensively takes into account the correlations between the heat generated during rock-breaking and several key factors, including the drill bit size, weight on bit, rotational speed, and the friction coefficient between the drill bit and the formation.

$$Q_{\rm rg} = \frac{fWN \left(D_{\rm g}^2 + D_{\rm g}^2 d_{\rm g} + d_{\rm g}^2\right)}{74.3 \left(D_{\rm g}^2 + d_{\rm g}\right)} \tag{12}$$

3.3.4. Calculation method for drilling fluid density and viscosity

Viscosity and density are crucial thermal properties of the drilling fluid. When analyzing the wellbore temperature field, to enhance computational efficiency, the circulating drilling fluid is typically assumed to have a constant density and constant viscosity. This assumption significantly simplifies the complexity of temperature field calculations. However, for ultra-deep wells with depths exceeding 10,000 m, the temperature and pressure conditions in different sections of the wellbore vary remarkably. As a result, the thermal properties of the drilling fluid change according to the environmental temperature and pressure of each well section, and these changes in thermal properties, in turn, can affect the heat transfer characteristics of the drill string and modify the wellbore temperature distribution.

During the circulation of the drilling fluid, viscosity serves as a key factor influencing energy transfer and fluid flow resistance. Under the large temperature and pressure variations in ultra-deep wells, the viscosity of the drilling fluid changes substantially. This leads to a significant variation in the Re of the circulating fluid, which further impacts the friction factor and alters the characteristics of the wellbore temperature distribution. The change in drilling fluid density mainly adjusts the wellbore temperature distribution by changing the specific heat capacity and heat transfer properties of the circulating fluid. Drilling fluid with a higher density has a higher specific heat capacity, enabling it to absorb and store more heat during the circulation process. Consequently, this reduces the rate of temperature change at the bottomhole. Additionally, an increase in fluid density also results in greater flow resistance of the circulating drilling fluid, thereby changing its heat transfer characteristics with the drill string and having an impact on the wellbore temperature distribution.

Specifically, as the drilling depth increases, the wellbore temperature ascends, triggering thermal expansion of the drilling fluid. This thermal expansion gives rise to a reduction in both the viscosity and density of the fluid. Consequently, the *Re* increases, making the fluid more prone to transitioning into a turbulent state. This turbulent flow enhances heat exchange across all regions of the wellbore. Meanwhile, the wellbore pressure also escalates with depth, intensifying the intermolecular interactions within the circulating fluid. This results in an elevation of the drilling fluid's viscosity, and the density increases due to compression effects, leading to a decrease in *Re*. This suppression of turbulence

subsequently diminishes heat exchange in various wellbore regions.

Regarding the relationship between drilling fluid viscosity and environmental temperature and pressure, the Andrade equation (Yan et al., 2022) is employed to characterize the decrease in drilling fluid viscosity as the temperature rises. Additionally, the Barus equation (Hermoso et al., 2017) is referenced to depict the increase in viscosity with increasing pressure. The empirical formula illustrated in Eq. (13) comprehensively describes the variation of drilling fluid viscosity with temperature and pressure.

$$\mu(T,P) = \mu_0 \exp\left(\beta \left(\frac{1}{T} - \frac{1}{T_0}\right) + \gamma(P - P_0)\right)$$
(13)

Analogously, the relationship between the drilling fluid density and the wellbore environmental temperature and pressure can be elucidated using the empirical formula presented Eq. (14).

$$\rho(T, P) = \rho_0 (1 - \alpha_T (T - T_0) + \alpha_P (P - P_0)) \tag{14}$$

3.3.5. Heat flux calculation

In oil and gas well drilling operations, the heat flux calculation for the wellbore system is composed of two main components: the heat flux calculation for the drill string and that for the wellbore-wall.

The heat exchange process of the drill string encompasses three key aspects: convective heat transfer between the annular fluid and the outer wall of the drill string, conductive heat transfer from the outer wall to the inner wall of the drill string, and convective heat transfer between the inner wall of the drill string and the internal drilling fluid. With respect to the heat transfer between the annular fluid and the internal fluid of the drill string, under the given assumption conditions, this process can be considered as a heat exchange mechanism through a single-layer thermal resistance within an infinitely long cylindrical tube. The heat transfer process through the drill string system is depicted in Fig. 5.

The temperature differences between the circulating drilling fluid within the drill string and the inner wall, between the inner and outer walls of the drill string, and between the outer wall and the annular drilling fluid are expressed as follows:



Fig. 5. 3D schematic diagram of heat conduction of the drill string.

$$\begin{cases} T_{\rm in} - T_{\rm pi} = \frac{\phi_{\rm p}}{2\pi r_{\rm pi} h_{\rm pi} l} \\ T_{\rm pi} - T_{\rm po} = \frac{\phi_{\rm p}}{2\pi k_{\rm p} l} \ln \frac{r_{\rm po}}{r_{\rm pi}} \\ T_{\rm po} - T_{\rm a} = \frac{\phi_{\rm p}}{2\pi r_{\rm po} h_{\rm po} l} \end{cases}$$
(15)

The heat flux through the drill string can be obtained by summing the temperature differences of each part:

$$\phi_{p} = \frac{2\pi l (T_{\text{in}} - T_{\text{a}})}{\frac{1}{r_{\text{pi}}h_{\text{pi}}} + \frac{1}{k_{\text{p}}} \ln \left(\frac{r_{\text{po}}}{r_{\text{pi}}}\right) + \frac{1}{r_{\text{po}}h_{\text{po}}}}$$
(16)

In Eq. (16), when calculating the heat flux through a unit length of the drill string, $l=1\,\mathrm{m}$.

The heat exchange process in the wellbore-wall system consists of two parts: convective heat transfer between the annular fluid and the wellbore-wall, and heat conduction from the wellbore-wall to the constant temperature boundary of the formation. Similarly, the wellbore-wall system can be regarded as a multi-layer cylindrical wall composed of three different thermal resistances: casing, cement, and formation. The heat transfer through the wellbore-wall is illustrated in Fig. 6. Eq. (17) provides the calculation method for heat exchange between the internal wellbore and the formation through the wellbore-wall, and the temperature difference calculations between each layer are omitted here for brevity.

$$\phi_{\rm C} = \frac{2\pi l (T_{\rm a} - T_{\rm OFT})}{\frac{1}{r_{\rm cl}h_{\rm cl}} + \frac{1}{k_{\rm c}} \ln \frac{r_{\rm co}}{r_{\rm cl}} + \frac{1}{k_{\rm ce}} \ln \frac{r_{\rm ceo}}{r_{\rm ce}} + \frac{1}{k_{\rm f}} \ln \frac{r_{\rm oFT}}{r_{\rm ceo}}}$$
(17)

When calculating the heat flux through the wellbore-wall for open-hole sections, the thermal resistance of the casing and cement is not considered. In addition, since the convective heat transfer coefficient between the annular fluid and the wellbore-wall is primarily influenced by factors such as annular size, fluid velocity, and flow conditions, this coefficient is still denoted as $h_{\rm Ci}$.

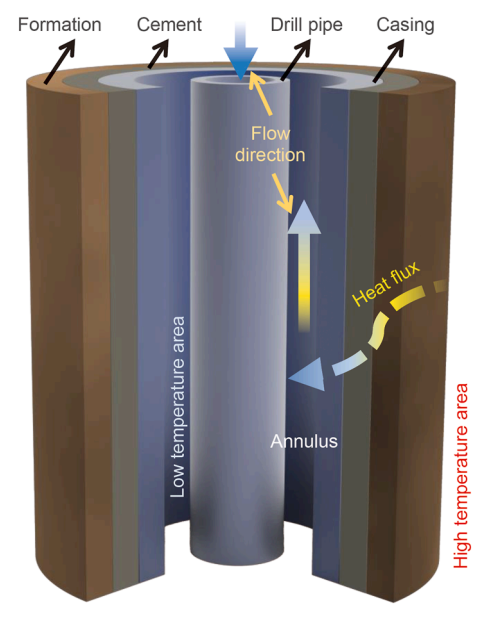


Fig. 6. 3D schematic diagram of heat conduction of the wellbore-wall.

The heat flux calculation formula for open-hole sections of the wellbore-wall is expressed as follows:

When calculating the heat flux through the wellbore-wall in open-hole sections, the thermal resistances of the casing and cement are excluded from consideration. Additionally, although the convective heat transfer coefficient between the annular fluid and the wellbore-wall is predominantly influenced by factors such as annular geometry, fluid velocity, and flow regime, this coefficient is still denoted as $h_{\rm ci}$. The heat flux calculation formula for the open-hole sections of the wellbore-wall is expressed as follows:

$$\phi_{\rm c} = \frac{2\pi l (T_a - T_{\rm OFT})}{\frac{1}{r_{\rm cl} h_{\rm rl}} + \frac{1}{k_{\rm f}} \ln \frac{r_{\rm OFT}}{r_{\rm ceo}}}$$
(18)

3.4. Initial and boundary conditions

3.4.1. Initial conditions

In the wellbore, it is assumed that at the initial moment, the temperatures within the drill string, annulus, and adjacent formation are identical at the same depth. Specifically, at t=0:

$$T_{\text{OFT}} = T_{\text{c}} = T_{\text{a}} = T_{\text{p}} = T_{\text{pi}} \tag{19}$$

3.4.2. Boundary conditions

The temperature of the fluid injected into the wellbore at the drill string inlet can be directly measured by sensors; thus, the temperature boundary condition at the drill string inlet is:

$$T_{\rm p}(z=0,t) = T_{\rm in}$$
 (20)

At the bottomhole, since the drilling fluid flows through the drill bit nozzles into the annulus, the initial temperatures within the drill string and annulus at the bottomhole are assumed to be equal:

$$T_{\rm pi}(z=H,t) = T_{\rm p}(z=H,t) = T_{\rm a}(z=H,t)$$
 (21)

The formation temperature at a radial position far from the wellbore axis is set as the undisturbed OFT:

$$T_{\rm f}(z,r\to\infty,t) = T_{\rm OFT}(z,t=0) \tag{22}$$

4. Analysis and discussion

In the preceding section, the physical and mathematical models for solving the wellbore temperature and heat flux in ultra-deep wells were established. Through the solution of these models, the wellbore-formation temperature field and heat flux values can be obtained. In this section, numerical simulations are conducted based on the deployment of TIDP tools for thermal insulation of the drill string system. Using the wellbore temperature field model, different TIDP deployment strategies are analyzed to derive conclusions on their applicability.

4.1. Introduction of TIDP

Prior to numerical analysis, a brief overview of the TIDP is provided. To substantially reduce heat exchange between the internal and external environments of the drill string system, this study proposes the TIDP concept, which involves filling the drill string structure with insulating materials of extremely low thermal conductivity. The TIDP described herein comprises an inner tube, an outer tube, inner/outer tube male-female connectors, and sealing elements. Due to the radial dimensional difference between the inner and outer tubes, a sealed annular gap is formed between them. By filling this gap with low-thermal-conductivity materials and applying thermal insulation coatings to the inner tube's outer wall and the outer tube's inner wall, the thermal conductivity of a single drill pipe is significantly reduced. This minimizes the impact of the high-temperature annular environment on the drill string's internal temperature during drilling operations.

Regarding the selection of insulating materials, this study considered the complex downhole environmental requirements and selected polyimide self-foaming material. This material features low thermal conductivity, a wide service temperature range, low density, excellent vibration resistance, and high-temperature durability, fully adapting to harsh downhole conditions. Polyimide is a class of polymers with imide rings in their main chains. The polyimide sample used in the annular gap of the TIDP in this study is designated as PI-66.6%-BPDA-G. To accurately simulate the wellbore temperature distribution and heat transfer characteristics of the drill string under TIDP deployment, the thermal conductivity of the polyimide sample (with a thickness consistent with the annular gap) was measured using the transient plane source technique and a DRE-III thermal conductivity tester. The test results showed that the thermal conductivity of the polyimide material in the TIDP annular gap was 0.04539 W/(m·°C), confirming its excellent thermal insulation performance. The structure of the TIDP, polyimide foam filling, and scanning electron microscope (SEM) schematic are shown in Fig. 7.

Additionally, due to the excellent sealing performance of the annular gap, the selection of the thermal insulation coating for the outer wall of the TIDP inner tube and the inner wall of the outer tube does not need to account for the high-temperature, high-pressure, corrosion, and erosion conditions within ultra-deep wellbore environments. This significantly expands the range of available coating materials. Currently, the thermal conductivity of existing 1 mm nano-porous coating materials can even reach below $0.02 \ \text{W/(m·°C)}$ (Lou et al., 2023). By combining the drill pipe with the insulating material, the overall thermal conductivity of a single TIDP can be reduced to as low as $0.03 \ \text{W/(m·°C)}$.

4.2. Model validation

In the absence of field application cases or downhole data for TIDP to validate the model directly, an alternative verification approach is adopted. Given that the primary distinctions between TIDP and CDP lie in their thermal conductivity and structural

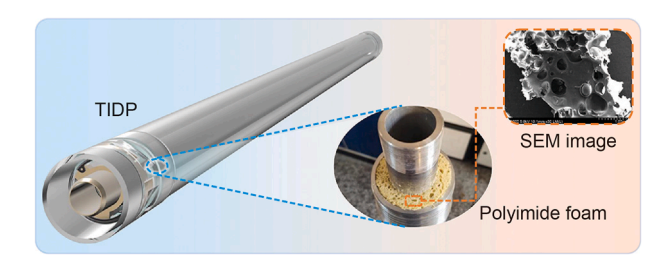


Fig. 7. Schematic diagram of the TIDP structure and polyimide insulation material filling.

parameters, the model's accuracy is validated by simulating the wellbore temperature field under full-CDP deployment conditions. This baseline validation leverages existing CDP datasets to ensure the model can accurately capture fundamental heat transfer mechanisms. Subsequently, the model is adapted to simulate TIDP scenarios by systematically adjusting parameters such as thermal conductivity, geometric dimensions, and deployment intervals. This parametric adjustment strategy enables efficient extension of the model's predictive capabilities to TIDP deployments, thereby bridging the gap between available validation data and the target application while ensuring both rigor and flexibility in evaluating the model's performance across different drill pipe systems.

Specifically, measurement while drilling (MWD) data from the ultra-deep slim-hole Well X in the Shunbei block in China was applied (Liu et al., 2024). The well's second section reaches a depth of 6750 m, with a surface temperature of 30 °C and an average geothermal gradient of 0.019 °C/m, water-based mud was used with a density of 1650 kg/m³, plastic viscosity of 27 mPa·s, and circulation rate of 32 L/s. As shown in Fig. 8, the calculated results from the proposed model agree closely with MWD-measured temperatures between 3000 and 5000 m depth. The temperature errors between simulation and measurement across this interval are < 3%, confirming the model's high accuracy in predicting wellbore temperature fields for ultra-deep wells.

4.3. Basic input parameters

To comprehensively characterize the temperature field and heat transfer characteristics of the wellbore-formation system, the basic input parameters are determined according to actual formation parameters and simulation requirements. Table 1 lists the relevant basic input parameters.

4.4. TIDP deployment methods for wellbore temperature control

Based on the five distinct TIDP deployment methods proposed in Section 2.3 and the basic parameter settings in Section 4.3, the drilling process of a 12,000 m well is used as a case study to illustrate these deployments. Table 2 describes the five TIDP deployment schemes for the drill string system.

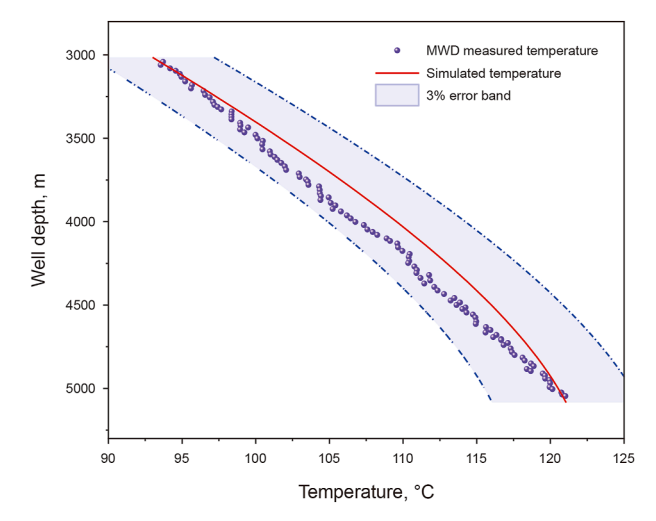


Fig. 8. Validation and error analysis of the wellbore temperature field model.

Table 1Basic input parameters for drilling operations.

Basic parameter	Value	Unit
Well depth	12,000	m
Drilling fluid inlet temperature	20	°C
Surface temperature	25	°C
Geothermal gradient	0.0197	°C/m
Circulation rate	60	L/s
Drilling fluid density	1500	kg/m ³
Formation rock density	2640	kg/m ³
Drilling fluid viscosity	15	mPa∙s
Drilling fluid thermal conductivity	1.75	W/(m⋅°C)
CDP thermal conductivity	43.75	W/(m⋅°C)
TIDP thermal conductivity	0.03	W/(m⋅°C)
Formation thermal conductivity	2.5	W/(m⋅°C)
Drilling fluid specific heat capacity	1600	J/(kg·°C)
Drill string specific heat capacity	400	J/(kg·°C)
Formation specific heat capacity	920	J/(kg·°C)

4.5. Study of wellbore thermodynamic characteristics

Based on the five TIDP deployment methods outlined in Section 4.4 and using the basic parameter settings, this section systematically investigates the thermodynamic characteristics of the wellbore through step-by-step analysis, focusing on the temperature distribution and heat transfer patterns within the wellbore-formation system. The goal is to identify optimal TIDP deployment strategies for the drill string system to guide practical drilling operations.

At the initial moment, it is assumed that the radial formation temperature is uniform at each depth. As drilling fluid circulates in the wellbore, the system gradually approaches thermal equilibrium with the adjacent formation. According to the first law of thermodynamics, once thermal equilibrium is reached, macroscopic temperature fluctuations in the wellbore and formation subside. By analyzing the temperature field and heat transfer behaviors under equilibrium conditions, the five TIDP deployment methods are evaluated to determine the most effective strategy.

Before investigating the TIDP deployment methods, it is essential to analyze the temporal evolution of the wellbore-formation temperature field and the impact of drilling fluid circulation on temperature distributions at various points within the wellbore-formation system. The aim is to determine the radial distance to the OFT boundary and the duration required for drilling fluid circulation to reach thermal equilibrium. These insights serve as the foundation for subsequent research and analysis in this section, with results integrated into the discussion in Section 4.5.1.

4.5.1. Method A

In Method A, TIDP are deployed throughout the entire wellbore, with the full-well deployment of CDP serving as the control group. This direct comparison enables the most intuitive observation of how TIDP installation affects the wellbore's thermodynamic characteristics.

Variation patterns of wellhead and bottomhole temperatures with circulation time

The annulus outlet temperature (AOT) and BHT can be directly measured using surface sensors and near-bit MWD instruments, respectively. Their fluctuations with drilling fluid circulation time are pivotal for analyzing wellbore temperature distribution characteristics. Higher AOT and BHT values signify elevated risks for drilling operations and accelerated wear on drilling equipment.

Table 2 The five TIDP deployment methods.

Method	Well section
Method A	0–12,000 m
Method B	0–1000 m; 0–2000 m; 0–3000 m; 0–4000 m; 0–5000 m; 0–6000 m
Method C	11,000–12,000 m; 10,000–12,000 m; 9000–12,000 m;
	8000–12,000 m; 7000–12,000 m; 6000–12,000 m
Method D	2000–6000 m; 4000–8000 m; 6000–10,000 m;
	1000–2000 m & 3000–4000 m & 5000–6000 m & 7000–8000 m & 9000–10,000 m
Method E	0–1000 m & 11,000–12,000 m; 0–2000 m & 10,000–12,000 m; 0–3000 m & 9000–12,000 m; 0–4000 m & 8000–12,000 m; 0–5000 m & 7000–12,000 m

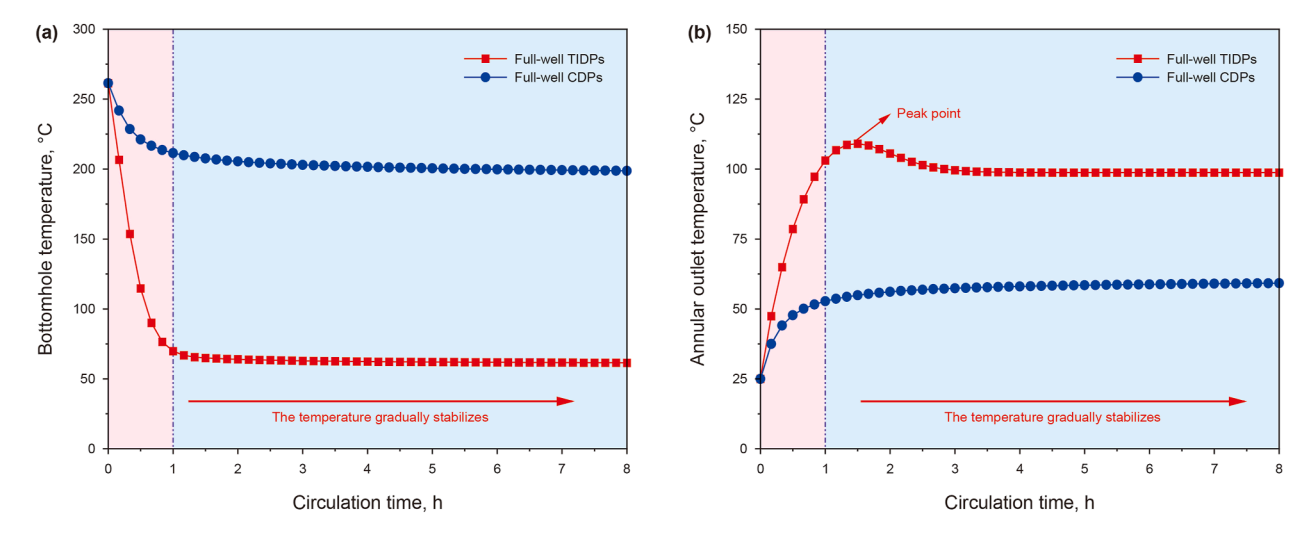


Fig. 9. Variation pattern of BHT and AOT with circulation time. (a) BHT, (b) AOT.

This section compares the temperature variations at the bottomhole and annulus outlet under continuous circulation, as depicted in Fig. 9. As shown in Fig. 9(a), full-wellbore deployment of TIDP significantly regulates the BHT. At the initial circulation stage, the BHT is approximately 261 °C, nearly equivalent to the formation temperature. During the first hour of drilling fluid circulation, the BHT experiences significant fluctuations, after which it gradually stabilizes.

In Fig. 9(b), the variation pattern of AOT over time under the condition of using CDP throughout the entire well is similar to that at the bottomhole. However, when TIDP is deployed throughout the entire well, the AOT first reaches a peak and then gradually stabilizes, showing a pattern distinct from that of using CDP. This difference can be explained as follows: on the one hand, due to the impact of TIDP, the heat exchange between the annular circulating fluid and the fluid inside the drill string is significantly weakened; on the other hand, the rate of radial heat transfer from the annulus to the adjacent formation is limited by the formation's thermal conductivity, causing gradual heat accumulation in the annulus outlet area and a rise in temperature until a peak is reached. At this point, the AOT is significantly higher than the fluid temperature inside the drill string and the radial formation temperature (as shown in the wellbore temperature distribution in Fig. 11 for the Method A), resulting in an extended transient heat exchange process in the drill string system and delaying the time needed for the annular fluid temperature to achieve thermal equilibrium. As the drilling fluid continues to circulate, heat is continuously transferred from the annulus outlet area to the adjacent formation. and the heat exchange process between the annular fluid, the formation, and the fluid inside the drill string gradually stabilizes, showing the variation pattern over circulation time as depicted in Fig. 9(b).

(2) Influence of drilling fluid circulation time on temperature at different locations

The near-bit area houses critical equipment such as MWD instruments, vertical drilling tools, and rotary steerable tools, which have limited tolerance to high temperatures. Excessively high BHT can cause malfunction or damage to these tools. Therefore, controlling BHT during drilling fluid circulation is a primary objective of wellbore temperature management. This section compares and analyzes temperature distribution patterns at the bottomhole and different radial positions in the formation for various circulation times, as shown in Fig. 10.

In Fig. 10(a), as the drilling fluid circulation time increases, the temperatures at different radial distances from the wellbore axis gradually stabilize. With the increase in radial distance, the degree of temperature variation for the same distance increment becomes progressively smaller, indicating that the influence of the wellbore temperature on the formation temperature diminishes with distance. Additionally, the closer to the wellbore axis, the more significant the temporal temperature variation and the shorter the time required to achieve thermal equilibrium. Conversely, the farther from the wellbore axis, the longer the equilibrium time. In the simulation analysis, the temperature coupling effect between wellbore fluid circulation and positions far from the wellbore axis is relatively weak and can be considered negligible. For research and numerical simulation purposes, a circulation time of 7 h is deemed sufficient for the wellbore-formation system to reach thermal equilibrium.

In Fig. 10(b), with the *x*-axis representing the radial distance from the wellbore axis, the radial temperature distribution at the bottomhole reveals that the rate of radial temperature variation in the wellbore decreases approximately linearly with increasing

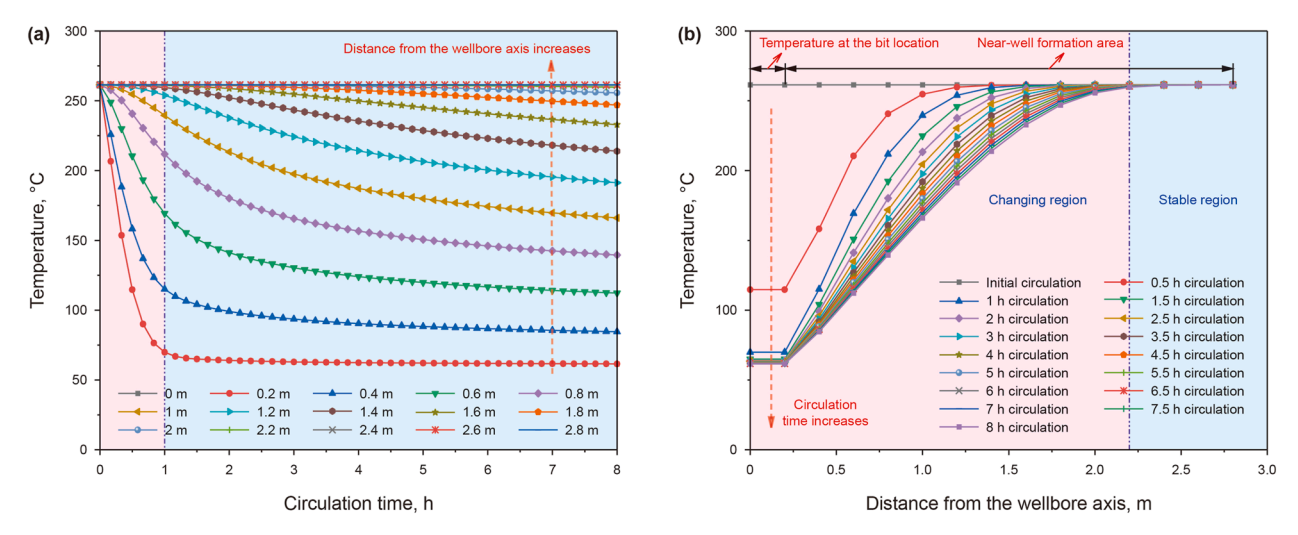


Fig. 10. Radial temperature variation pattern at different positions of the bottomhole with circulation time. (a) BHT at different circulation time, (b) BHT at different positions.

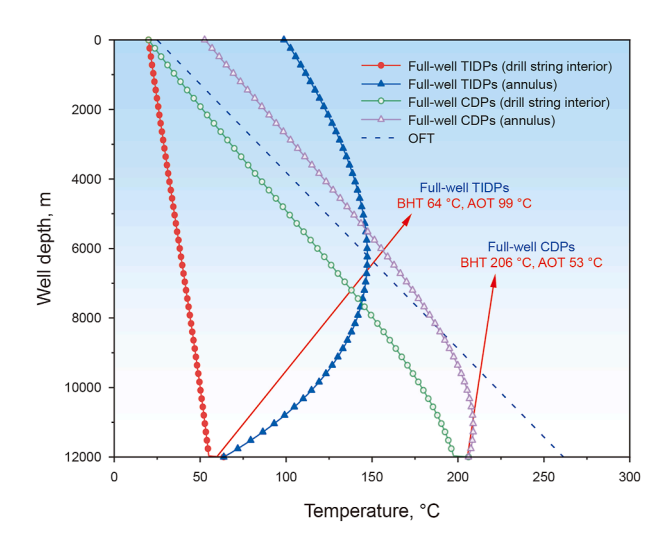


Fig. 11. Comparison of wellbore temperature distribution between full-well TIDP and CDP deployments.

distance from the wellbore axis. The temperatures inside the drill string and annulus (i.e., within the wellbore) change most rapidly with circulation time. As circulation continues, heat is rapidly transferred from the wellbore interior to the near-well formation. The figure indicates that wellbore temperature variations primarily affect the formation temperature within a radius of 1.2 m. With further increases in radial distance, the impact of the wellbore on formation temperature gradually diminishes. At a radial distance of 2.2 m from the wellbore axis, the formation temperature no longer changes with wellbore fluid circulation, which can be considered the point where the formation temperature is unaffected by circulating drilling fluid. For research and numerical simulation purposes, a radial distance of 2.2 m is defined as the boundary condition for the influence range of wellbore fluid circulation temperature. Beyond 2.2 m from the wellbore axis, the formation temperature is approximately equal to the OFT.

(3) Temperature distribution pattern of the wellbore under thermal equilibrium

The temperature distribution patterns of the wellbore under thermal equilibrium conditions for full-well TIDP and CDP deployments are shown in Fig. 11. When TIDP is deployed throughout the entire well, heat exchange between the drill string's internal drilling fluid and the high-temperature annular environment is significantly weakened due to the drill string system's low thermal conductivity. Under ideal conditions, the BHT with full-well TIDP deployment is only 64 °C, a reduction of over three times compared to the 206 °C BHT observed with CDP. Analyzing the temperature distribution of fluid flowing from the top to the bottom of the drill string, the internal temperature of the TIDP-deployed drill string exhibits an almost linear variation, differing from the pattern observed with CDP. Because TIDP significantly reduce the drill string system's thermal conductivity, the primary source of internal fluid temperature increase is frictional heat generation, with minimal heat transfer from the annulus through the drill string into the internal fluid. Consequently, except for minor nonlinear fluctuations, the overall temperature distribution follows a nearly linear heating trend.

According to the law of energy conservation, the total heat within the wellbore system does not spontaneously emerge or vanish. Owing to the low thermal conductivity of the drill string and wellbore-wall, heat in the annular fluid cannot be efficiently dissipated or timely transferred to other spatial regions, leading to a significant temperature rise as the drilling fluid flows from the annulus bottom to the surface. In Fig. 11, the AOT reaches 99 °C under full-well TIDP deployment, nearly double that under fullwell CDP deployment. When using TIDP, the highest temperature point in the wellbore shifts significantly upward to the midwellbore annular region, after which the temperature gradually decreases at a lower rate-markedly different from the conventional temperature distribution patterns in regular drilling operations. With TIDP deployment, the depth of the wellbore section where the annulus temperature equals the OFT moves upward by approximately 2000 m. This ensures that downhole tools, MWD instruments, and deep-well drilling equipment remain within a safe working temperature range, significantly prolonging the service life of downhole instruments and equipment, and thus achieving the economic and safety objectives of drilling operations.

The above research and analysis highlight the significance of simulating wellbore thermodynamic parameters using TIDP tools. Through a comprehensive investigation of thermodynamic conditions under different TIDP deployment methods, effective guidance can be provided for oilfield drilling engineering operations.

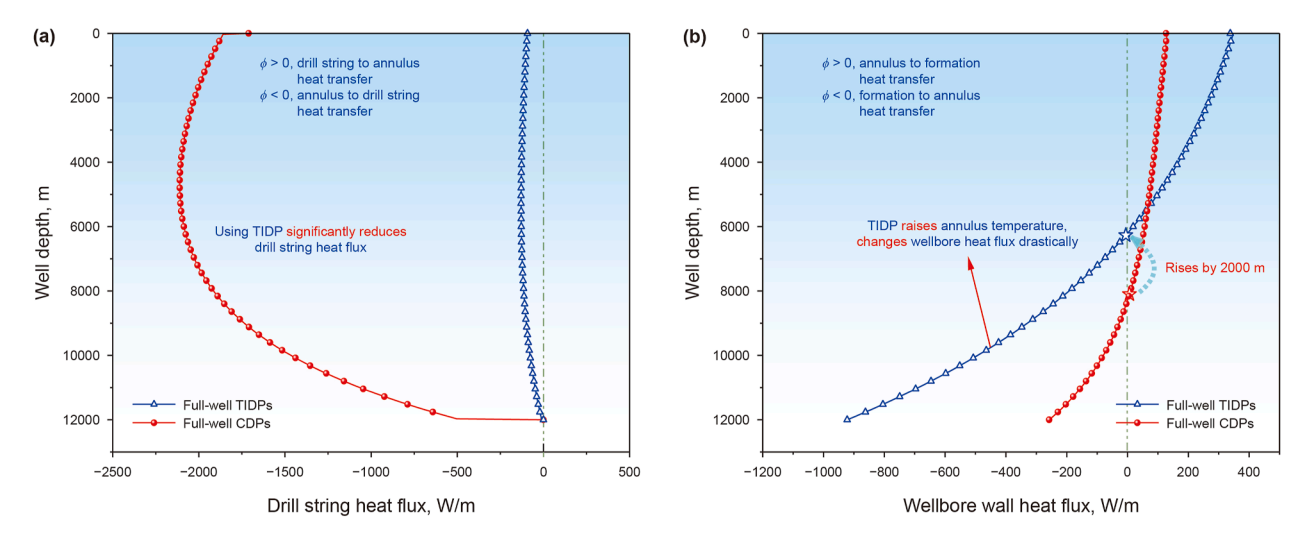


Fig. 12. Wellbore heat flux under Method A. (a) Drill string heat flux, (b) wellbore-wall heat flux.

The primary driver of wellbore temperature variation is the heat exchange between the circulating fluids in the drill string and annulus through the drill string and wellbore-wall systems. Fig. 12 compares the variation patterns of heat flux per unit length of the drill string for full-well TIDP and CDP deployments. A negative heat flux value signifies heat transfer from the annulus to the drill string, while a positive value indicates heat transfer from the drill string to the annulus. By analyzing the heat flux at different well depths in the drill string system, the characteristics of heat exchange between the drill string's internal fluid and the annulus under TIDP deployment are clearly revealed. At the bottomhole, where drilling fluid enters the annulus through the drill bit nozzle, the temperatures of the drill string's internal fluid, the drill string itself, and the annulus are equal. Observation shows that the heat flux at the bottomhole is zero, indicating no macroscopic heat exchange occurs at this location.

When comparing the heat flux at different positions within the wellbore-wall system, a negative heat flux value indicates heat transfer from the adjacent formation into the annulus through the wellbore-wall, while a positive value indicates heat transfer from the annulus to the formation. As shown in Fig. 12, replacing CDP with TIDP in the drill string system not only significantly reduces the heat flux through the drill string but also induces substantial changes in the wellbore-wall heat flux. Under TIDP conditions, the depth at which the wellbore-wall heat flux becomes zero has shifted upward by approximately 2000 m compared to the CDP condition. This means the well depth where the annulus temperature equals the formation temperature has moved upward by 2000 m, which aligns with the depth shown in Fig. 11 where the annulus and formation temperatures are equal.

In the analysis of this section, the radial distance within 2.2 m from the wellbore axis is defined as the influence range of the circulating temperature. To fully illustrate the variations in the wellbore and near-well formation temperature fields under TIDP deployment conditions, a visual representation of the wellformation temperature field is presented through temperature field heat distribution maps, as shown in Fig. 13. The positions of the drill string and the wellbore-wall are marked in the figure according to their respective distances from the wellbore axis. The advantages of using TIDP are clearly demonstrated: the temperature at the near-bottom position and the adjacent formation is significantly reduced, while the annulus temperature in the upper well section increases, and the temperature of the adjacent

formation rises accordingly. In subsequent analyses, to avoid added lines and text from affecting heat map comparisons, the positions of the drill string and the wellbore-wall will no longer be marked.

4.5.2. Method B

The wellbore temperature distribution for varying lengths and numbers of TIDP deployed continuously from the wellhead downward is compared, as shown in Fig. 14. In Fig. 14(a), the temperature distribution inside the drill string exhibits a distinct pattern: as the number of TIDP increases, the BHT gradually decreases, and the rate of decrease accelerates, indicating that deeper TIDP deployment enhances BHT reduction efficiency. Comparing the annulus temperature distribution in Fig. 14(b), a greater BHT decrease correlates with a higher AOT. Results show that Method B is less effective in reducing BHT. The primary cause is that after the drill string's internal fluid exits the TIDP-deployed section, heat exchange with the annulus significantly increases, diminishing the cooling effect achieved in the TIDP region.

Fig. 15 illustrates the heat flux distribution through the drill string system and the wellbore-wall system. Observation shows that due to the varying lengths of the TIDP-deployed sections, the heat flux through the drill string exhibits a sudden change at the transition points between TIDP and CDP. As the annular fluid flows past this point, the thermal resistance for heat transfer into the drill string significantly increases, causing a sudden rise in the heat flux transferred from the annulus to the adjacent formation through the wellbore-wall. After the fluid inside the drill string flows past this transition point, the heat exchange in the drill string system gradually stabilizes for different TIDP lengths, as indicated by the decreasing difference in heat flux values in the near-bottom region shown in Fig. 15(a), until the heat flux at the bottomhole reaches zero.

In Fig. 15(b), after the annular circulating fluid passes through the transition point, heat exchange with the drill string system decreases sharply. The annulus temperature is mainly affected by frictional heat from fluid flow and the formation temperature, gradually increasing until it exceeds the radial OFT at the same depth. At this stage, heat starts to transfer from the annulus to the formation through the wellbore-wall, showing the heat flux variation pattern depicted in Fig. 15(b).

The well-formation temperature heat distribution for Method B is shown in Fig. 16. As the length of TIDP deployment increases, the

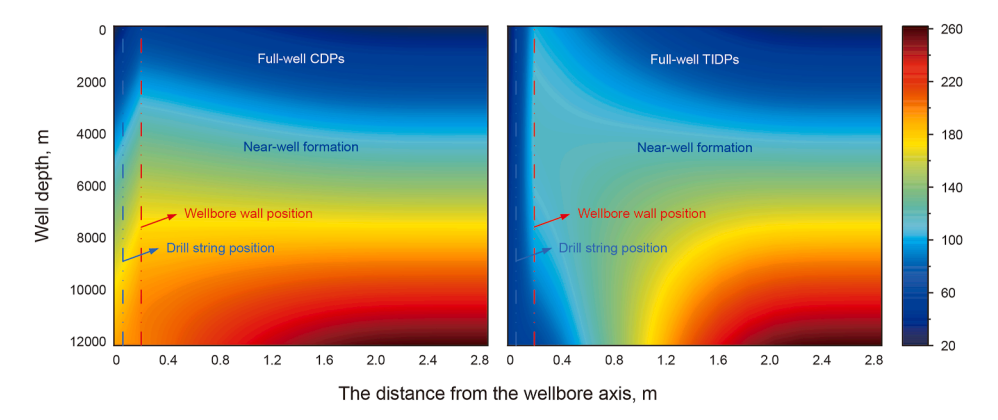


Fig. 13. Comparative heat distribution maps of wellbore-formation for Method A.

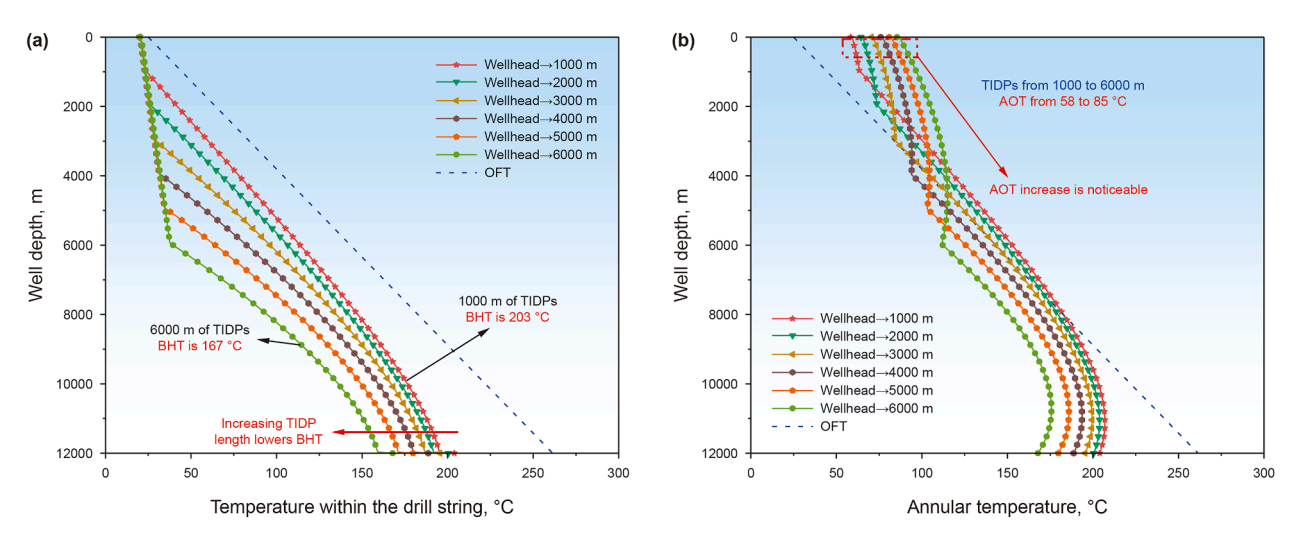


Fig. 14. Wellbore temperature distribution under Method B. (a) Temperature within the drill string, (b) annular temperature.

low-temperature region inside the drill string in the upper well section gradually expands, while the AOT rises progressively. Although the deep formation temperature decreases slightly due to the overall well temperature reduction, the change remains insignificant. This further confirms that Method B demonstrates suboptimal performance in regulating wellbore temperature.

4.5.3. Method C

As the number of TIDP gradually increases from the bottomhole upward, the BHT decreases progressively, as illustrated in Fig. 17. Under this TIDP deployment method, the AOT exhibits minimal variation. The primary reason lies in the fact that the AOT is predominantly influenced by the upper wellbore section. Owing to

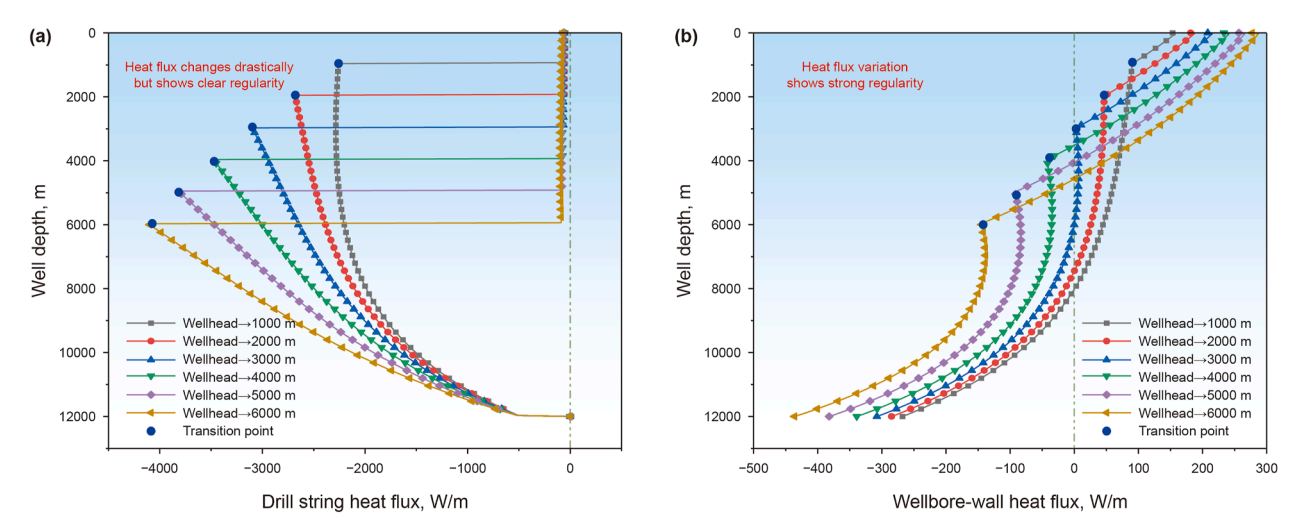


Fig. 15. Wellbore heat flux under Method B. (a) Drill string heat flux, (b) wellbore-wall heat flux.

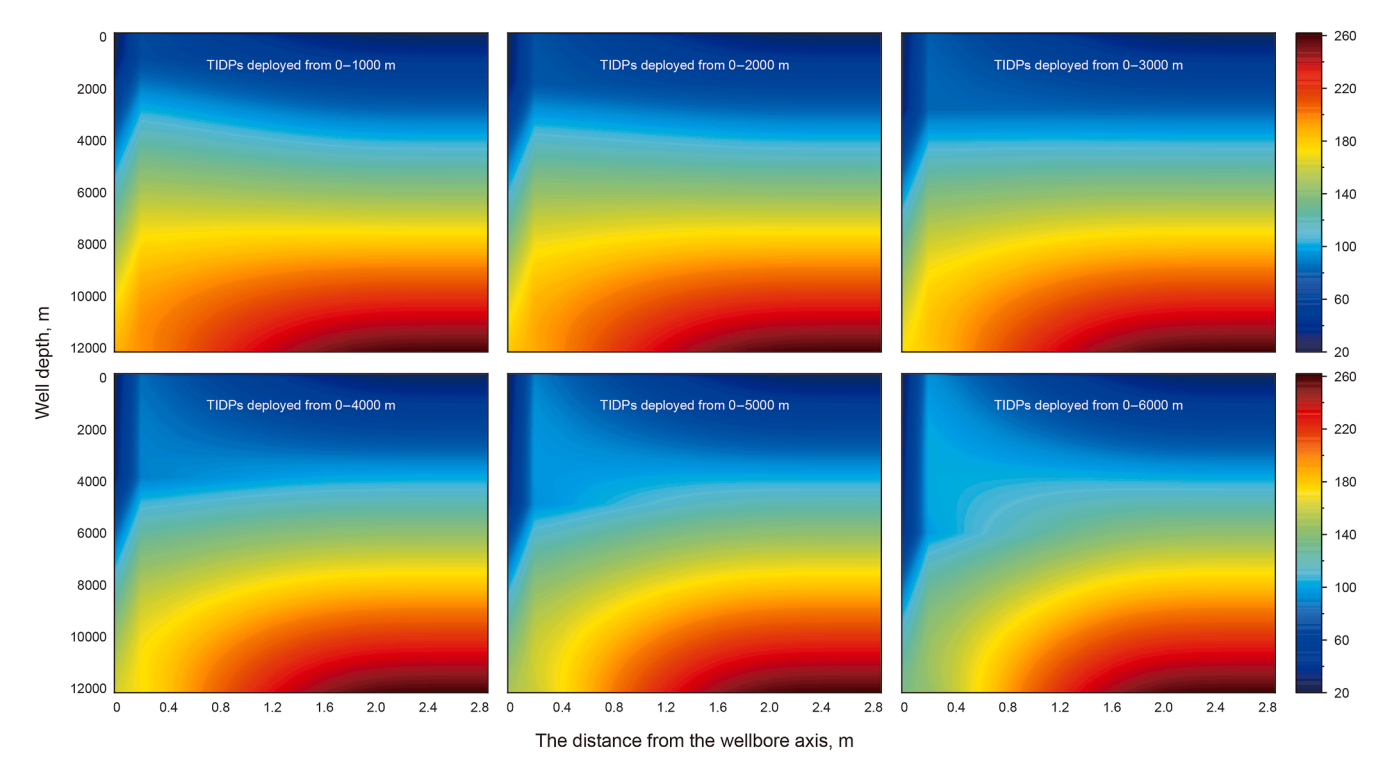


Fig. 16. Comparative heat distribution maps of wellbore-formation for Method B.

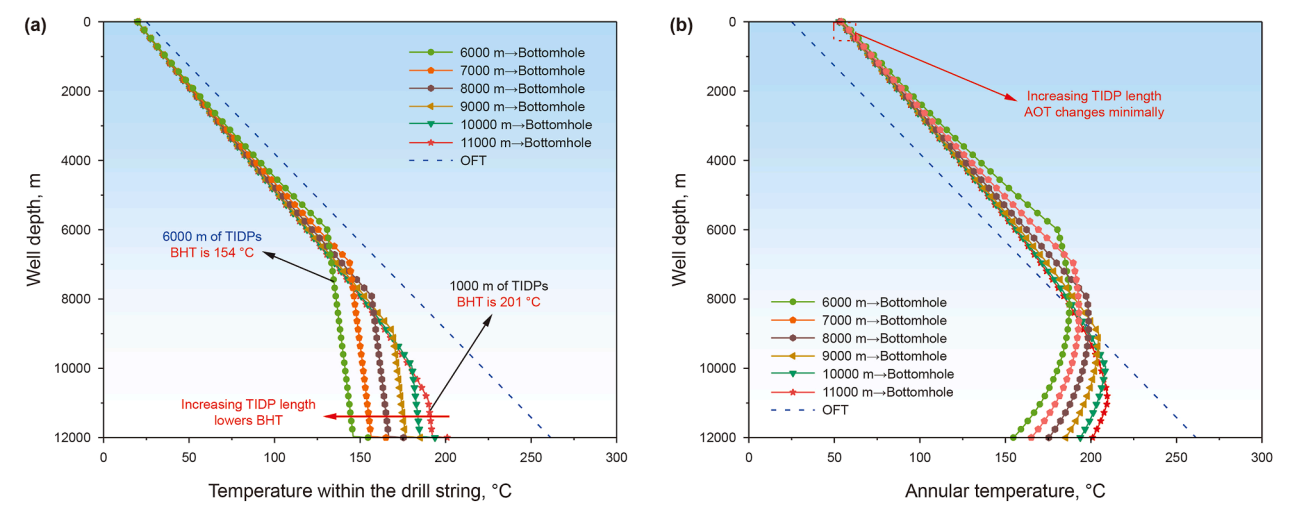


Fig. 17. Wellbore temperature distribution under Method C. (a) Temperature within the drill string, (b) annular temperature.

the prolonged convective heat transfer process involving the annular fluid, CDP, and wellbore-wall in the upper section, the impact of TIDP on the AOT is correspondingly diminished.

Fig. 18 presents the heat flux variation patterns of the drill string system for Method C. Similar to Method B, the heat flux through the drill string shows a sudden change at the TIDP-CDP connection point, as depicted in Fig. 18(a). When the annular circulating fluid flows past this transition point, heat exchange between the annulus and the internal drill string increases significantly. From the transition point to the annulus outlet, continuous heat exchange in the drill string system causes the heat flux values in the drill string and wellbore-wall for different TIDP lengths to gradually converge. This phenomenon is reflected in

Fig. 17, where the AOT difference under different TIDP lengths is minimal.

The well-formation temperature heat distribution pattern shown in Fig. 19 contrasts with the wellhead-down deployment method. When TIDP is progressively deployed upward from the bottomhole, the wellbore temperature in the near-bit area is effectively reduced. Concurrently, the temperature of the deep near-well formation decreases due to the influence of wellbore temperature variations, while the AOT remains largely unaffected.

Method C enables significant regulation of the BHT while keeping the AOT within a narrow range. Specifically, when deploying 6000 m of TIDP, the BHT reduces by 52 $^{\circ}$ C, while the AOT increases by only 1 $^{\circ}$ C. To comprehensively compare with Method

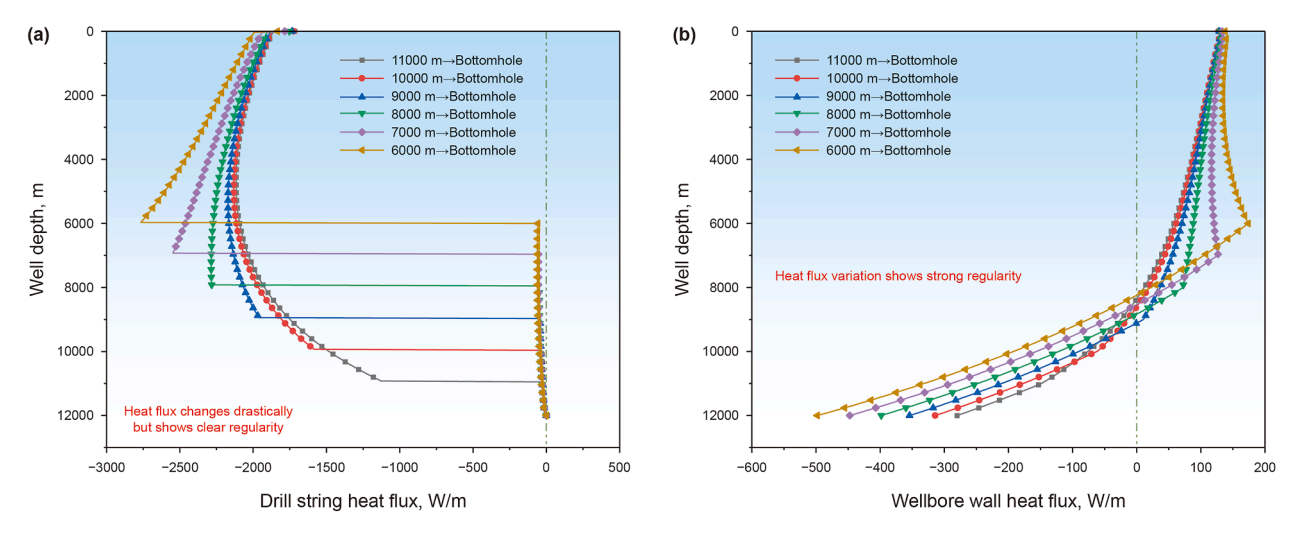


Fig. 18. Wellbore heat flux under Method C. (a) Drill string heat flux, (b) wellbore-wall heat flux.

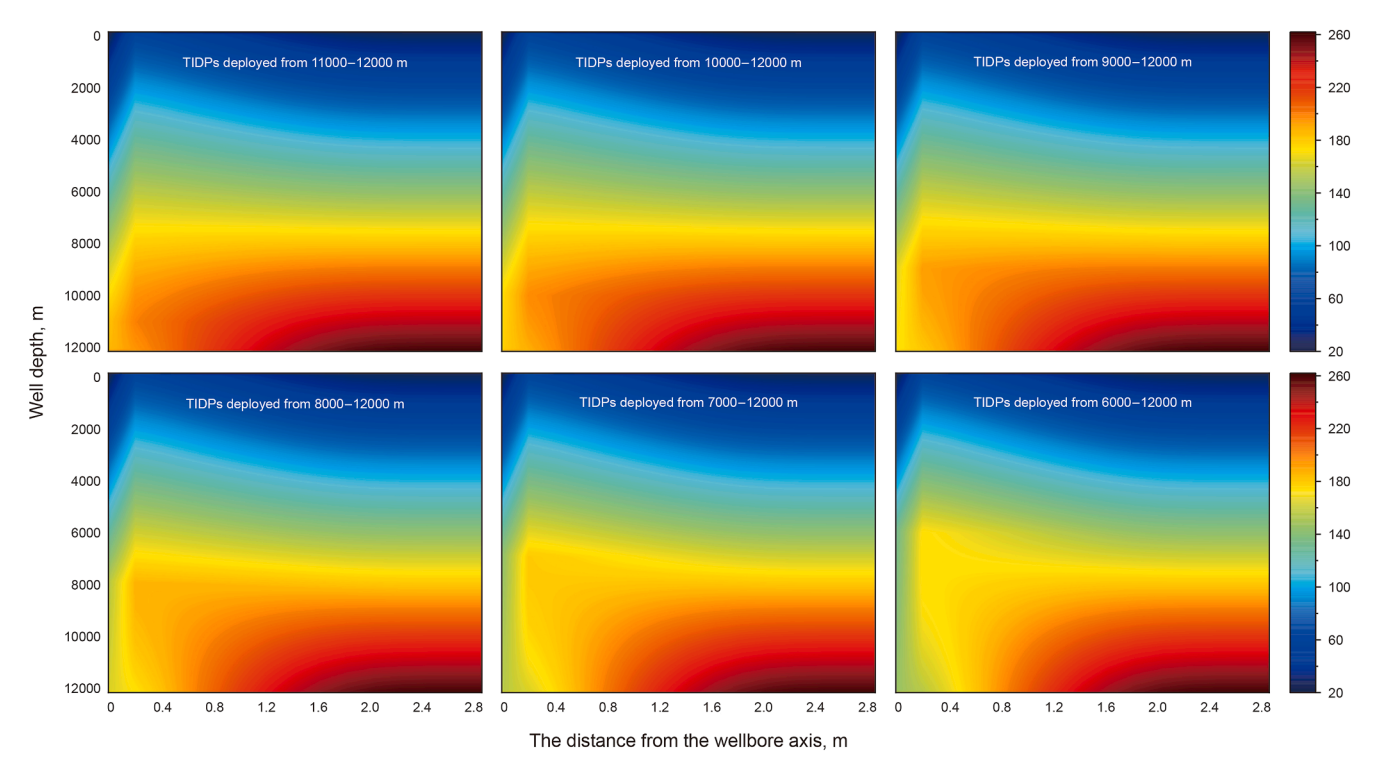


Fig. 19. Comparative heat distribution maps of wellbore-formation for Method C.

B and further validate the cooling effect of Method C, numerical simulations were supplemented by incrementally increasing the TIDP length by 1000 m from the bottomhole upward until the entire drill string was equipped with TIDP, as illustrated in Fig. 20. As the TIDP deployment length increases and the CDP section decreases, when the length of TIDP exceeds two-thirds of the well section, the amplitude of AOT variation grows, and the annulus temperature in the upper wellbore section gradually rises.

Based on the above analysis, TIDP deployment should prioritize the middle and deep well sections to maintain both the BHT and AOT at relatively low levels. This strategy balances bottomhole cooling and AOT control by concentrating thermal insulation on deeper zones where high temperatures pose the most significant risk to downhole tools, while simultaneously preventing excessive

heat accumulation at the annulus outlet, and thus ensuring the safety and stability of near-bit temperature-sensitive instruments (e.g., MWD tools, rotary steerable systems) and ground-based drilling fluid cooling equipment.

4.5.4. Method D

In this section, TIDP is deployed in the middle well section, with the resulting wellbore temperature distribution shown in Fig. 21. Adjusting the position and length of TIDP deployment in the middle section reveals that Method D has minimal impact on the wellhead and BHT due to the presence of CDP at both the top and bottom ends of the drill string system. The placement of TIDP in the middle well section significantly alters the temperature distribution within the drill string and annulus, reshaping the high-

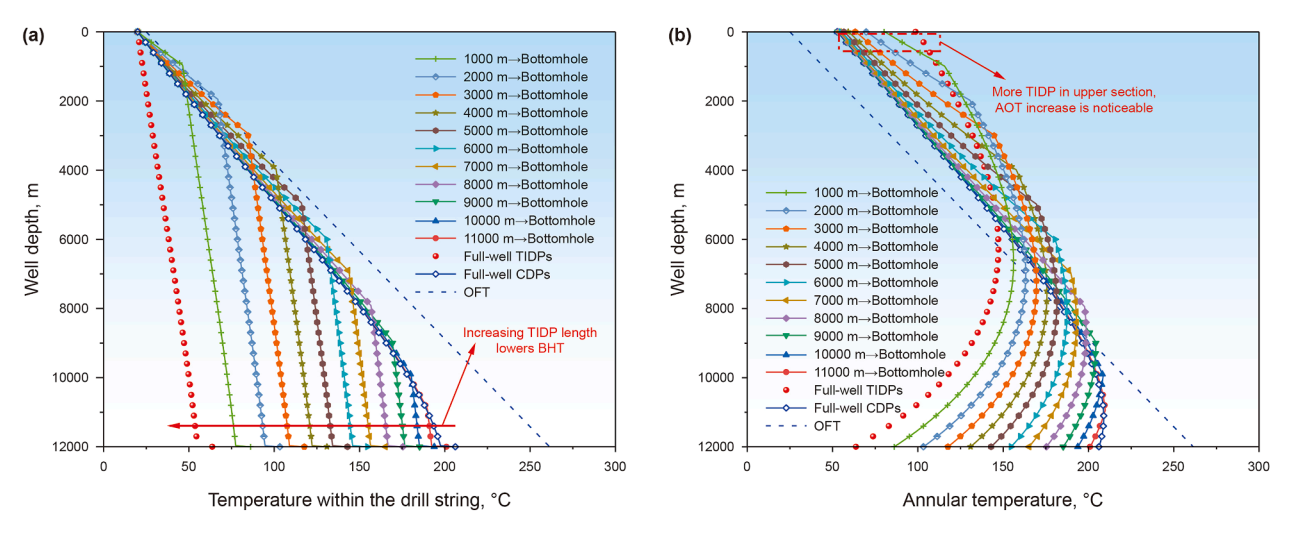


Fig. 20. Supplementary simulation of wellbore temperature distribution under Method C. (a) Temperature within the drill string, (b) annular temperature.

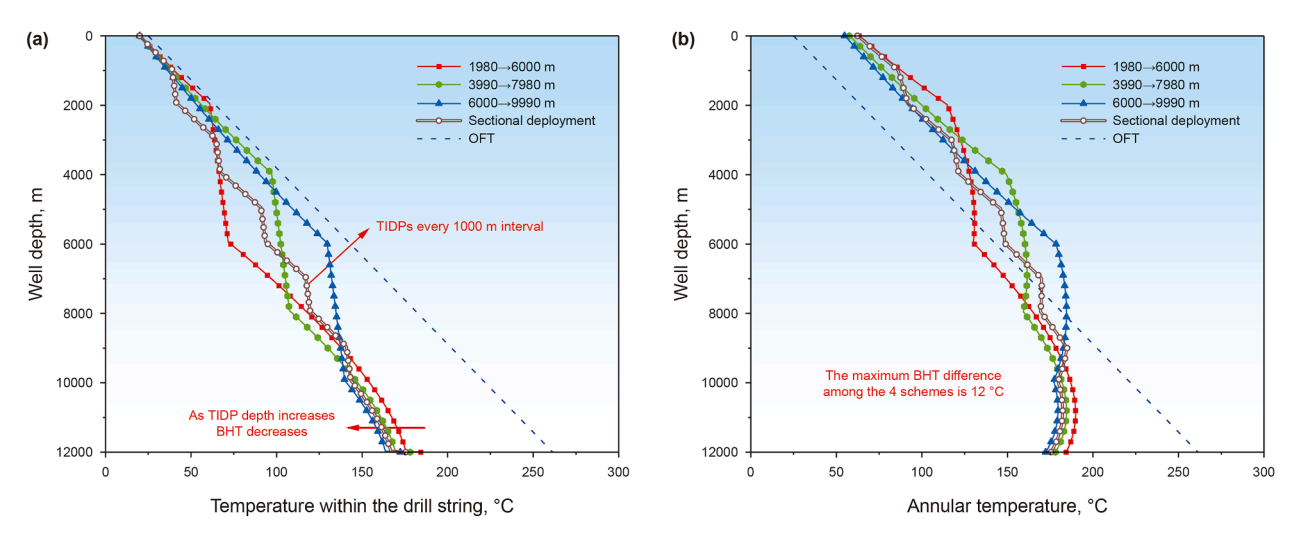


Fig. 21. Wellbore temperature distribution under Method D. (a) Temperature within the drill string, (b) annular temperature.

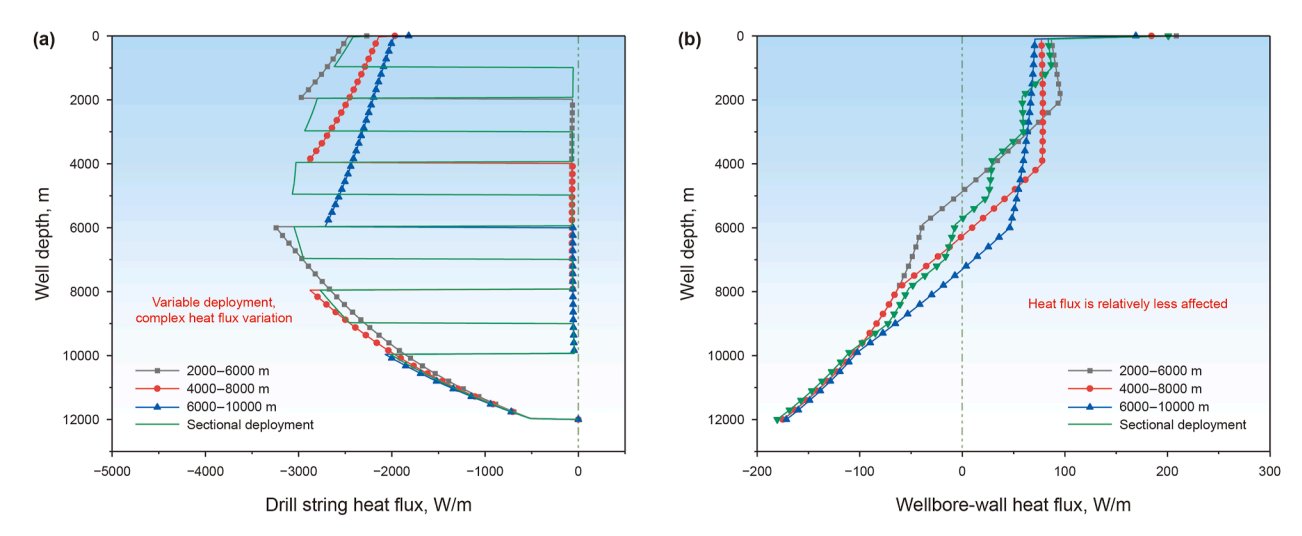


Fig. 22. Wellbore heat flux under Method D. (a) Drill string heat flux, (b) wellbore-wall heat flux.

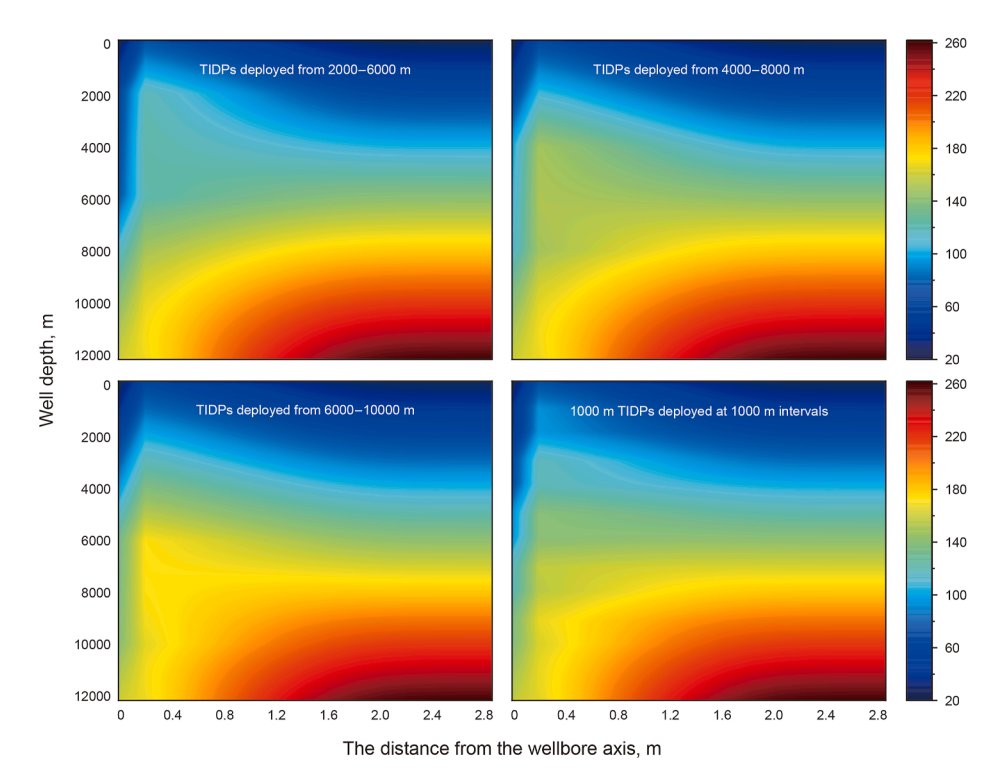


Fig. 23. Comparative heat distribution maps of wellbore-formation for Method D.

temperature region in the annulus. In practical engineering applications, deploying TIDP near intelligent short sections or measurement tools with temperature-sensitive components ensures that the temperature in these areas is regulated within a predetermined safe range. This targeted deployment balances thermal insulation efficiency with overall wellbore heat management, preventing overheating of critical downhole equipment while minimizing interference with temperature dynamics at both ends of the wellbore.

When TIDP is deployed in the middle well section, the heat flux through the drill string system undergoes drastic changes, particularly in segmented TIDP deployments, which exhibit multiple heat flux transition points, as illustrated in Fig. 22.

Owing to variations in heat flux through the drill string, the heat flux through the wellbore-wall system also shifts with the location of these transition points, thereby modifying the temperature variation trend of the circulating fluid in the annulus. These abrupt changes in heat flux at TIDP-CDP interfaces reflect altered thermal resistance and heat transfer efficiency. Such alterations directly influence how heat is distributed between the drill string, annulus, and surrounding formation. The resulting annulus temperature dynamics highlight the complex interplay between localized thermal insulation (via TIDP) and broader heat exchange processes in the wellbore, underscoring the importance of strategic TIDP placement for optimizing temperature control in targeted sections.

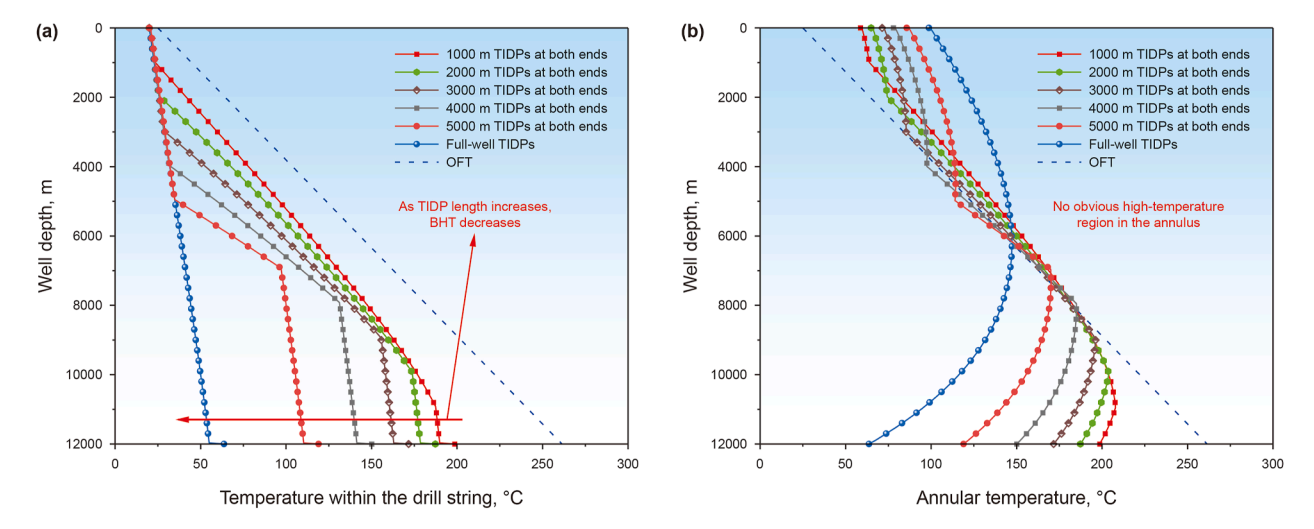


Fig. 24. Wellbore temperature distribution under Method E. (a) Temperature within the drill string, (b) annular temperature.

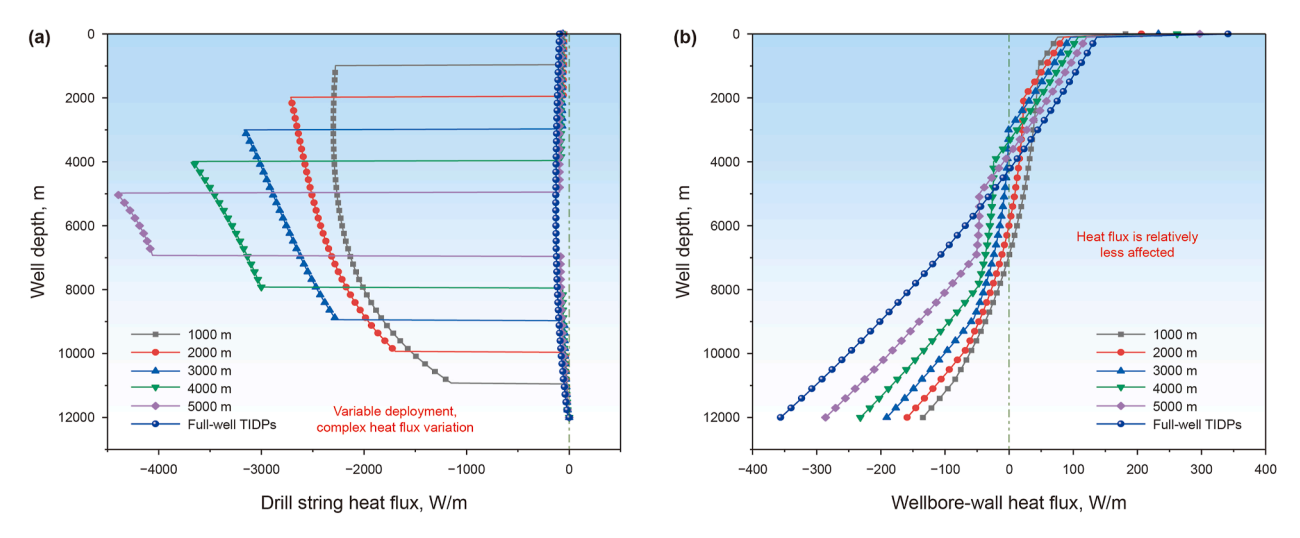


Fig. 25. Wellbore heat flux under Method E. (a) Drill string heat flux, (b) wellbore-wall heat flux.

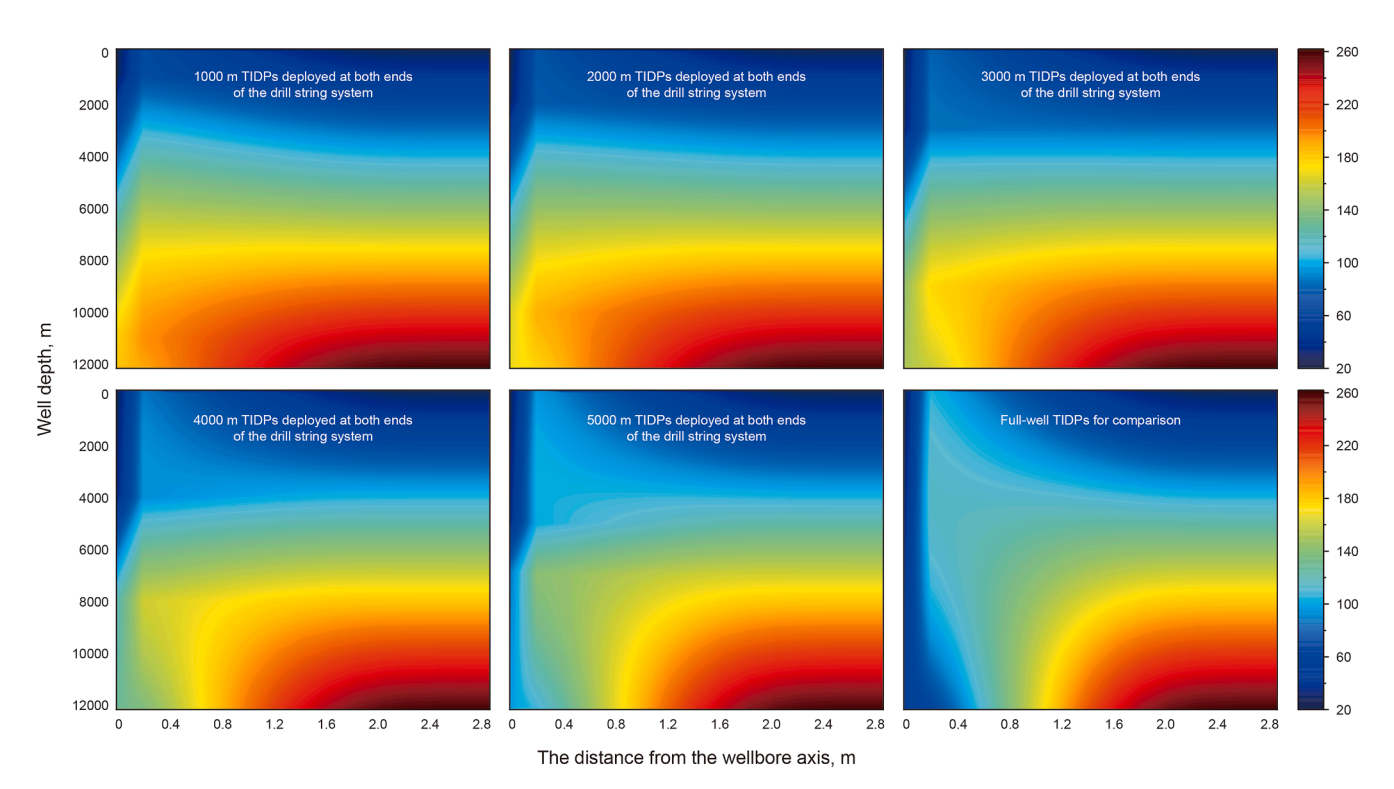


Fig. 26. Comparative heat distribution maps of wellbore-formation for Method E.

As shown in Fig. 23, the effect of TIDP on well temperature regulation is relatively limited; consequently, the impact of the wellbore temperature on the adjacent formation remains confined. Simulation results indicate that Method D is primarily employed to control localized high-temperature regions in the wellbore, tailored to specific deployment locations.

This targeted approach highlights the utility of TIDP in addressing thermal hotspots near critical downhole equipment (e. g., measurement tools or intelligent short sections) without significantly altering the broader temperature dynamics of the entire wellbore or surrounding formation.

4.5.5. Method E

In previous sections, the temperature distribution and heat flux patterns of the wellbore for four different methods were simulated. To provide a more intuitive comparison of the changes in wellbore temperature distribution in the upper and lower well sections and the heat transfer characteristics of the drill string system, this section presents the case of deploying TIDP at both ends of the drill string system. Specifically, an equal number of TIDP are deployed simultaneously from the wellhead downward and from the bottomhole upward within a certain range. The resulting wellbore temperature distribution is shown in Fig. 24.

Observation shows that this deployment method maintains the annular circulation temperature in the middle well section close to the OFT. Compared with other TIDP deployment methods, this method achieves better control of high temperatures in the wellbore, keeping the annular circulation temperature throughout the well section consistently within a relatively low range.

The heat flux variation patterns are similar to those in other deployment methods, as shown in Fig. 25. As the number of TIDP at both ends of the drill string system increases, the temperature difference between the internal fluid in the CDP-deployed section and the annulus gradually widens. As seen in Fig. 25(a), the heat flux in the CDP-deployed section rises significantly, even exceeding 4000 W/m.

The well-formation temperature distribution for Method E, as shown in Fig. 26, demonstrates a significant alteration in the temperature distribution of the near-well formation. As the number of TIDP increase, the well temperature is uniformly and stably controlled within a relatively low range.

As shown in Fig. 26, the well-formation temperature distribution for Method E reveals a notable modification in the temperature profile of the near-well formation. With an increase in the number of TIDP, the wellbore temperature is uniformly and stably regulated within a relatively low range.

4.6. Applicability discussion

The simulation studies in Section 4.5 are completed, and the applicability of the five TIDP deployment methods is analyzed as follows:

Full-well TIDP deployment (Method A) achieves the best cooling effect at the bottomhole, but its extensive use of TIDP leads to relatively high costs. Moreover, the reduction in BHT results in significant heat accumulation in the annulus, causing a notable rise in the outlet temperature. This imposes higher demands on the performance of ground drilling fluid cooling equipment. Additionally, as introduced in Section 4.1, TIDP features a nested double-tube structure—while the polyimide insulation material in the annular gap has a relatively low density, the total weight of the drill string system in ultra-deep drilling operations exceeding 10,000 m is much greater than that of CDP, significantly increasing the operational load on ground top drive equipment.

Wellhead-down TIDP deployment (Method B) is affected by the high-temperature environment of the deep near-well formation, causing the temperature of the drilling fluid circulating in the wellbore to rise significantly and resulting in less effective wellbore temperature control. Therefore, this method is not recommended for comprehensive well temperature regulation.

Bottomhole-up TIDP deployment (Method C) can significantly regulate the wellbore temperature near the drill bit while keeping the AOT from becoming excessively high, making it the optimal solution for controlling near-bit well temperatures. However, it should be noted that as the number of TIDP increases, the temperature inside the CDP-deployed sections of the drill string also rises, and the heating rate of the annulus outlet gradually accelerates. Thus, for Method C, the number of TIDP should be reasonably planned, with a focus on deployment in the middle and deep well sections. This approach ensures effective cooling while reducing TIDP usage and lowering the operational burden on ground cooling equipment, balancing the economic feasibility of drilling operations with cooling requirements to achieve optimal drilling performance.

Middle well section TIDP deployment (Method D) does not achieve satisfactory temperature regulation at the wellhead and bottomhole but can effectively control the temperature in the TIDP-deployed region. For example, in well sections equipped with intelligent short sections or MWD tools, deploying TIDP in the

adjacent drill string system can regulate the heating rate in the target region, thereby preventing damage to temperature-sensitive instruments caused by high wellbore temperatures and extending the service life of such equipment.

Dual-end TIDP deployment (Method E) achieves better overall control of high-temperature regions along the entire wellbore. As shown in the simulations in Section 4.5.5, this method maintains the annulus temperature in the middle and deep well sections close to the OFT, ensuring no significant high-temperature zones exist throughout the wellbore.

In wellbore temperature control, adjusting the BHT to a level far below the maximum tolerance of temperature-sensitive instruments is inconsistent with the economic requirements of drilling operations. Additionally, such temperature reduction increases the operational load on ground top drives and cooling equipment, shortening the service life of related tools and equipment and resulting in significant waste of engineering resources. Therefore, in ultra-deep drilling operations, it is essential to select a suitable TIDP deployment method based on specific wellbore temperature control requirements and actual drilling conditions. A comprehensive evaluation should consider economic efficiency, cooling performance, and targeted cooling regions to ensure effective temperature control in ultra-high-temperature deep formations.

4.7. Research advantages and limitations

This paper presents a comprehensive theoretical model for calculating ultra-deep wellbore temperatures, systematically investigating dynamic temperature changes under five distinct TIDP deployment methods in the drill string system, quantitatively analyzing complex heat transfer mechanisms in ultra-long wellbores, and establishing methodologies for TIDP application in drilling. Compared to existing models, this new model fully integrates the impacts of multiple factors on wellbore temperature, including: circulating drilling fluid flow friction, variable geothermal gradients, heat generated by drill-bit rock-breaking, and variations in drilling fluid density and viscosity with temperature-pressure environments. Leveraging an advanced finite element solution, the study accurately characterizes wellbore temperature dynamics and heat transfer laws in ultra-long well sections under drill pipe insulation conditions, enabling high-precision simulations to guide TIDP scheme design and optimization for ultra-high-temperature drilling environments.

While this work provides a robust theoretical framework, the model was developed under idealized assumptions regarding TIDP performance, downhole environments, and fixed parameters. In practical drilling operations, TIDP may experience structural damage, thermal insulation degradation, or failure due to ultrahigh temperature/pressure, corrosion, erosion, acidification, or prolonged downhole service. Therefore, future research on downhole drill string insulation should prioritize experimental and field testing of circulating fluid temperature regulation, TIDP damage detection, and performance evaluation under complex conditions to refine model accuracy and optimize TIDP deployment strategies.

5. Conclusions

This work established a wellbore temperature field model for ultra-deep wells, based on which the temperature distribution of the wellbore-formation and the downhole heat exchange patterns for five different TIDP deployment methods were analyzed and compared. The main conclusions are listed as follows:

- (1) Significant thermal conductivity differences exist between TIDP and CDP in the drill string system. When using TIDP, the heat flux in the drill string system is significantly reduced, effectively suppressing heat exchange between the annulus and the drill string. This reduces the heating rate of fluids inside the drill string, enabling active control of the temperature of drilling fluid circulating in the wellbore.
- (2) Different TIDP deployment methods exhibit remarkable variations in downhole temperature field regulation. Overall, deploying TIDP from the bottomhole toward the wellhead demonstrates optimal comprehensive temperature control performance. By arranging TIDP in the middle and deep well sections, this method not only meets the stringent temperature control requirements near the drill bit in ultradeep high-temperature environments but also maintains the annulus outlet drilling fluid temperature at a relatively low level
- (3) The core of wellbore temperature control via TIDP lies in reconstructing downhole high-temperature zones. Through appropriate TIDP deployment strategies, the hightemperature zones originally concentrated at the bottomhole are shifted to non-critical areas. This maintains the temperature environment of near-bit temperature-sensitive instruments (e.g., intelligent subs, MWD) within safe thresholds, addressing the challenge of "thermal hazards concentrating at the tool end" in ultra-deep drilling.
- (4) Simulation results of the five deployment methods show that TIDP can precisely regulate heat flux distribution in the drill string system, controlling wellbore temperature within the target range for safe drilling. This breaks through the exploration bottleneck of traditional drilling in formations with temperatures exceeding 150 °C. The technology is expected to push drilling depths beyond 10,000 m, providing critical technical support for the large-scale development of ultra-high-temperature deep resources.

CRediT authorship contribution statement

Heng-Rui Zhang: Writing - review & editing, Writing - original draft, Software, Project administration. Yi-Nao Su: Methodology, Conceptualization. Mao-Lin Liao: Funding acquisition, Data curation. Hong-Yu Wu: Supervision, Investigation. Hai-Yan Zhang: Investigation. Hao-Yu Wang: Validation. Ke Liu: Resources, Project administration.

Declaration of competing interest

The authors declare that they have no known competing financial interests or personal relationships that could have appeared to influence the work reported in this paper.

Acknowledgements

This research work was supported by the National Natural Science Foundation of China (Grant No. U22B2072) and Research Project of China Petroleum Science and Technology Innovation Fund (Grant No. 2025DQ02-0144).

Nomenclature		
t	Time step.	
Q_{rg}	Heat from drill bit-formation friction, J.	
$r_{\rm pi}$	Inner radius of drill string, m.	
$r_{\rm po}$	Outer radius of drill string, m.	
$r_{\rm ci}$	Inner radius of casing, m.	
$r_{\rm co}$	Outer radius of casing, m.	
$r_{ m f}$	Inner radius of formation control volume, m.	
$r_{\rm ceo}$	Outer radius of cement, m.	
$r_{ m cei}$	Inner radius of cement, m.	
Z	Height of control volume, m.	
С	Specific heat capacity (drilling fluid), J/(kg·°C)	
c_{f}	Specific heat capacity (formation), J/(kg·°C)	
$c_{\rm p}$	Specific heat capacity (drill string), J/(kg·°C)	
h_{pi}	Drill string inner wall-drilling fluid convective heat	
1.	transfer coefficient, W/(m ² ·°C)	
h_{po}	Drill string outer wall-annular fluid convective heat	
1.	transfer coefficient, W/(m²·°C) Heat transfer coefficient (inner wall of the wellbore),	
h_{ci}	$W/(m^2 \cdot C)$	
L.	Axial thermal conductivity (drill string), W/(m^2 ·°C)	
$k_{\rm p}$ $k_{\rm c}$	Thermal conductivity (casing), $W/(m^2 \cdot C)$	
$k_{\rm f}$	Thermal conductivity (casing), $W/(m^2 \cdot c)$	
k_{ce}	Thermal conductivity (rement), $W/(m^2 \cdot C)$	
T Ce	Ambient temperature, °C	
P	Ambient pressure, °C	
$T_{\rm in}$	Temperature (drilling fluid inside the drill string), °C	
$T_{\rm a}$	Temperature (annular drilling fluid), °C	
$T_{\rm p}$	Temperature (drill string), °C	
$T_{\rm OFT}$	Original formation temperature, °C	
$T_{ m f}$	Temperature of the near-well formation control	
	volume, °C	
T_0	Surface temperature, °C	
G_{i}	Geothermal gradient of different formation types, °C/m	
$v_{\rm in}$	Flow velocity (drilling fluid inside the drill string), m/s	
$v_{\rm a}$	Flow velocity (annular fluid), m/s	
P_0	Surface pressure, Pa	
D	Diameter of flow channel, m.	
$L_{\rm i}$	Depth corresponding to geothermal gradients, m.	
Nu	Nusselt number	
D_{h}	Hydraulic diameter, m.	
$D_{ m g}$	Outer diameter of the drill bit, m.	
$d_{ m g}$	Inner diameter of the drill bit, m.	
l	Well section length, m.	
W	Weight on bit, N.	
N	Rotational speed, rpm	

Greek letters

 f_s

ϵ	Absolute roughness of the inner wall of the pipe or
	annulus, m.
α_{i}	Inclination angle of the well
λ	Thermal conductivity of the medium, W/(m.°C)
ρ	Density of the drilling fluid, kg/m ³
$\rho_{ m p}$	Density of the drill string, kg/m ³
$\rho_{\rm f}$	Density of the near-well formation, kg/m ³
μ	Viscosity of the drilling fluid, mPa·s

Drill pipe heat flux, W.

Friction factor of the selected medium

Friction coefficient between the drill bit and the

- $\phi_{\rm c}$ Wellbore-wall heat flux, W.
- β Temperature sensitivity coefficient
- γ Pressure sensitivity coefficient
- α_{T} Thermal expansion coefficient
- α_p Volumetric compressibility coefficient

References

- An, J., Li, J., Huang, H., et al., 2023. Numerical study of temperature-pressure coupling model for the horizontal well with a slim hole. Energy Sci. Eng. 11, 1060–1079. https://doi.org/10.1002/ese3.1370.
- Edwardson, M.J., Girner, H.M., Parkison, H.R., et al., 1962. Calculation of formation temperature disturbances caused by mud circulation. J. Petrol. Technol. 14 (4), 416–426. https://doi.org/10.2118/124-PA.
- Finger, J.T., Jacobson, R.D., Champness, A.T., 2002. Development and testing of insulated drillpipe. SPE Drill. Complet. 17, 132–136. https://doi.org/10.2118/ 78267-PA.
- Fénot, M., Bertin, Y., Dorignac, E., et al., 2011. A review of heat transfer between concentric rotating cylinders with or without axial flow. Int. J. Therm. Sci. 50 (7), 1138–1155. https://doi.org/10.1016/j.ijthermalsci.2011.02.013.
- Fu, J., Su, Y., Jiang, W., et al., 2019. Research and application of wellbore transient temperature in deep shale gas horizontal wells. Journal of Southwest Petroleum University (Science & Technology Edition) 41 (6), 165–173 (in Chinese).
- Hasan, A.R., Kabir, C.S., 1992. Two-phase flow in vertical and inclined annuli. Int. J. Multiphas. Flow 18 (2), 279–293. https://doi.org/10.1016/0301-9322(92)
- Hermoso, J., Martinez-Boza, F.J., Gallegos, C., 2017. Modeling pressure-viscosity behavior of oil-based drilling fluids. Oil & Gas Science and Technology–Revued IFP Energies Nouvelles 72 (4), 18. https://doi.org/10.2516/ogst/2017014.
- Kabir, C.S., Hasan, A.R., Kouba, G.E., et al., 1996. Determining circulating fluid temperature in drilling, workover, and well control operations. SPE Drill. Complet. 11 (2), 74–79. https://doi.org/10.2118/24581-PA.
- Kohei, A., Naganawa, S., Bjarkason, E., 2023. Application of insulated drill pipe to supercritical/super-hot geothermal well drilling, Proceedings of the ASME 2023 42nd International Conference on Ocean, Offshore and Arctic Engineering. Volume 9: Offshore Geotechnics; Petroleum Technology. https://doi.org/ 10.1115/OMAE2023-104713.
- Lou, F., Dong, S., Zhu, K., et al., 2023. Thermal insulation performance of aerogel nano-porous materials: characterization and test methods. Gels 9, 220. https:// doi.org/10.3390/gels9030220.
- Liu, T., He, M., Zhang, Y., et al., 2024. Research on wellbore temperature prediction model and cooling method of ultra deep well with small hole. Drill. Prod. Technol. 47 (3), 65–67 (in Chinese).
- Memarzadeh, F.D., Stefan, Miska, 1984. Numerical Simulation of diamond-bit Drilling with Air. SPE Rocky Mountain Regional Meeting. https://doi.org/10.2118/12908-MS.
- Michaelides, E., 2006. Particles, bubbles and drops: their motion, heat and mass transfer. World Scientific.
- Mohamed, S.K., Chen, D.M., Pradeepkumar, A., et al., 2023. Drilling heat maps for active temperature management in geothermal wells. SPE J. 28, 1577–1593. https://doi.org/10.2118/210306-PA.
- Mao, L., Wei, C., Zeng, S., et al., 2023. Heat transfer mechanism of cold-water pipe in ocean thermal energy conversion system. Energy 269, 126857. https://doi. org/10.1016/j.energy.2023.126857.
- Petersen, J., Bjørkevoll, K.S., Lekvam, K., 2001. Computing the Danger of Hydrate Formation Using a Modified Dynamic Kick Simulator. IADC Drilling Conference. https://doi.org/10.2118/67749-MS.

- Peng, Q., Fan, H., Zhou, H., et al., 2016. Drilling Fluid Density Calculation Model at High Temperature High Pressure. Offshore Technology Conference Asia. https://doi.org/10.4043/26620-MS.
- Qiu, M., Ostfeld, A., Avi, O., 2021. A head formulation for the steady-state analysis of water distribution systems using an explicit and exact expression of the colebrook-white equation. Water 13, 1163. https://doi.org/10.3390/w13091163
- Ramey, H.J., 1962. Wellbore heat transmission. J. Petrol. Technol. 14 (4), 427–435. https://doi.org/10.2118/96-PA.
- Raymond, L.R., 1969. Temperature distribution in a circulating drilling fluid. J. Petrol. Technol. 333–341. https://doi.org/10.2118/2320-PA.
- Rao, B.K., 2000. Heat transfer to non-newtonian flows over a cylinder in cross flow. Int. J. Heat Fluid Flow 21 (6), 693–700. https://doi.org/10.1016/S0142-727X(00) 00063-1
- Schlumberger, C., Schlumberger, M., Leonardon, E.G., 1934. Electrical coring; a method of determining bottom-hole data by electrical measurements. OR Trans. 110, 237–272. https://doi.org/10.2118/934237-G.
- Swamee, P.K., Jain, A.K., 1976. Explicit equations for pipe-flow problems. J. Hydraul. Div. 102 (5), 657–664. https://ascelibrary.org/doi/10.1061/JYCEAJ.0004542.
- Song, X., Guan, Z., 2011. Full transient analysis of heat transfer during drilling fluid circulation in deep-water wells. Acta Pet. Sin. 32 (4), 704–708 (in Chinese).
- Saeed, S., 2012. Gene expression programming analysis of implicit colebrook—white equation in turbulent flow friction factor calculation. J. Petrol. Sci. Eng. 92–93, 48–55. https://doi.org/10.1016/j.petrol.2012.06.005.
- Song, X., Yao, X., Xu, Z., et al., 2024. Research on the influence mechanism of heatinsulating coating parameters in temperature-controlled drilling of ultra-deep well. Petroleum Drilling Techniques 52 (2), 126–135 (in Chinese).
- Wang, H., Shen, Z., Li, G., 2011. Influences of formation water invasion on the well bore temperature and pressure in supercritical CO₂ drilling. Petrol. Explor. Dev. 38 (3), 362–368. https://doi.org/10.1016/S1876-3804(11)60039-6.
- Wang, K., Liu, B., Zhang, J., et al., 2019. Calculation and analysis of wellbore temperature field in HTHP gas wells. China Petroleum Machinery 47 (1), 8–13 (in Chinese).
- Xiao, D., Hu, Y., Meng, Y., et al., 2022a. Research on wellbore temperature control and heat extraction methods while drilling in high-temperature wells. J. Petrol. Sci. Eng. 209, 109814. https://doi.org/10.1016/j.petrol.2021.109814. Xiao, D., Hu, Y., Wang, Y., et al., 2022b. Wellbore cooling and heat energy utilization
- Xiao, D., Hu, Y., Wang, Y., et al., 2022b. Wellbore cooling and heat energy utilization method for deep shale gas horizontal well drilling. Appl. Therm. Eng. 213, 118684. https://doi.org/10.1016/j.applthermaleng.2022.118684.
- Xiao, D., Xiao, H., Song, W., et al., 2024. Utilization method of low-grade thermal energy during drilling based on insulated drill pipe. Renew. Energy 225, 120363. https://doi.org/10.1016/j.renene.2024.120363.
- Yan, Q., Liu, S., Liu, C., et al., 2022. Research status and prospects of cavitation characteristics of viscous oil. J. Mech. Eng. 1–18 (in Chinese).
- Yang, H., Li, J., Zhang, H., et al., 2022a. Numerical analysis of heat transfer rate and wellbore temperature distribution under different circulating modes of reelwell drilling. Energy 254 (B), 124313. https://doi.org/10.1016/j.energy.2022. 124313
- Yang, H., Li, J., Zhang, H., et al., 2022b. Thermal behavior prediction and adaptation analysis of a reelwell drilling method for closed-loop geothermal system. Appl. Energy 320, 119339. https://doi.org/10.1016/j.apenergy.2022.119339.
- Zhang, H., Su, Y., Liao, M., et al., 2025. Thermal management of drilling fluids with phase change materials in ultra-high temperature wells. Appl. Therm. Eng. 274 (Part A), 126601. https://doi.org/10.1016/j.applthermaleng.2025.126601.
- Zhang, W., Xu, Z., Lyu, Z., et al., 2023. Research on a transient flow heat transfer model of gas-liquid-solid three-phase flow for unbalanced drilling in deep shale wells. Petroleum Drilling Techniques. 51 (5), 96–105 (in Chinese).